

# INSTABILITY OF EQUILIBRIA FOR THE 2D EULER EQUATIONS ON THE TORUS

HOLGER DULLIN, ROBERT MARANGELL AND JOACHIM WORTHINGTON

*School of Mathematics and Statistics, Carlaw Building (F07),  
The University of Sydney, NSW 2006*

*Email: Joachim.Worthington@sydney.edu.au (corresponding author),  
Holger.Dullin@sydney.edu.au, Robert.Marangell@sydney.edu.au*

ABSTRACT. The hydrodynamics of an incompressible fluid can be approximated as a finite dimensional Hamiltonian system by a truncation introduced by Zeitlin [21, 22]. With periodic boundary conditions, there exists a family of stationary solutions with vorticity  $\Omega^* = 2\Gamma \cos(\mathbf{p} \cdot \mathbf{x})$ . Zeitlin's truncation is used to analyse the linear stability of these solutions and compare this with a Galerkin truncation. Following Li's [12] method the problem is divided into subsystems and we prove that most subsystems are linearly stable. We derive a sufficient condition for a subsystem to be linearly unstable and derive an explicit lower bound for the associated real eigenvalues independent of the truncation size  $N$ . This together with known stability results for the 2D periodic Euler equations allows us to show that most of these stationary solutions are nonlinearly unstable. We confirm our results this with numerical computation of the spectrum for a finite truncation. Finally we discuss the essential spectrum of the full problem as the limit of the truncated problem.

## 1. INTRODUCTION

In terms of the vorticity  $\Omega(\mathbf{x}, t) : (\mathbb{T}^2 \times \mathbb{R}^+) \rightarrow \mathbb{R}$ , the 2D incompressible Euler equations are (see [2] Appendix 2 for an overview)

$$(1.1) \quad \frac{\partial \Omega}{\partial t} + u_1 \frac{\partial \Omega}{\partial x_1} + u_2 \frac{\partial \Omega}{\partial x_2} = 0, \quad \frac{\partial u_1}{\partial x_1} + \frac{\partial u_2}{\partial x_2} = 0.$$

Here  $\mathbf{x} = (x_1, x_2)^T$  and  $u_1, u_2$  are the velocity components in the  $x_1$  and  $x_2$  directions respectively. We impose periodic boundary conditions  $\Omega(\pi, x_2, t) = \Omega(-\pi, x_2, t)$  and  $\Omega(x_1, \pi, t) = \Omega(x_1, -\pi, t)$ . There is a family of stationary solutions given by

$$(1.2) \quad \Omega^* = 2\Gamma \cos(\mathbf{p} \cdot \mathbf{x})$$

for  $\Gamma \in \mathbb{R}$  and  $\mathbf{p} \in \mathbb{Z}^2$ .

The study of stability of certain solutions of the planar Euler equations was initiated by Arnol'd's seminal work [1] on the Lie-Poisson structure of the Euler equations where he invented the Energy-Casimir method to prove stability. This is revisited in Arnol'd and Khesin [3], in particular Section II.4. Arnol'd discusses a slightly more general problem where the torus has dimensions  $X \times 2\pi$  and  $\mathbf{p} = (0, 1)^T$ , and shows that this solution is non-linearly stable when  $X \leq 2\pi$ . In [14] it was shown that any equilibrium with

$\mathbf{p} = (0, 1)^T$  and  $X > 2\pi$  is linearly unstable for the viscous problem using linear stability analysis and infinite continued fractions. That paper also shows linear instability for  $\mathbf{p} = (0, m)^T$ ,  $m > 1$  and any  $X$ . The linear instability of the inviscid problem for  $\mathbf{p} = (0, m)^T$ ,  $m > 1$  was proved in [5] and discussed in [6]. Under the condition  $m^2 \neq m_1^2 + m_2^2$  for any positive integers  $m_1, m_2$ , it was shown in [8] that the steady state for  $\mathbf{p} = (0, m)^T$  is nonlinearly unstable.

Li [12] showed how to block-diagonalise the linearisation about the equilibrium with general  $\mathbf{p}$  into so-called ‘classes’, and using this approach he again showed that  $p = (0, 1)^T$  is Lyapunov stable. Latushkin et al [11] study the essential and discrete spectrum of the linearisation of (1.1) at the steady state (1.2). They study the full infinite system and approach the problem from a functional analysis perspective. There, an upper bound on the number of non-imaginary isolated eigenvalues is given, and the essential spectrum is described. Furthermore, they show that the spectrum of the linearised operator is the union of the spectrum coming from each of the classes from [12] and they show that the spectral mapping theorem holds for the Euler operator linearised about  $\Omega^*$  (Theorem 2 in [11]).

In the viscous problem solutions  $e^{-\nu m^2 t} \cos(mx)$  are called *bar states* in [4]. They show that for non-zero viscosity  $\nu$ , and  $m = 1$  these bar states are ‘quasi-stationary’, in that they decay on a slow timescale depending on the viscosity.

We combine the block-diagonalisation used by Li with Zeitlin’s [21] structure preserving finite-dimensional truncation to prove that for a large class of  $\mathbf{p}$  the stationary solutions (1.2) are nonlinearly unstable. Zeitlin’s truncation leads to a finite dimensional Poisson structure and hence the Hamiltonian structure of the original PDE and its Casimirs are preserved in the finite-dimensional problem. See [3] and [10] for a discussion of the use of Poisson brackets in hydrodynamics.

In Section 2, the problem and the associated notation are introduced. The system is first decomposed into Fourier modes which are described by a non-canonical infinite dimensional Hamiltonian system. Then Zeitlin’s truncation is used to reduce to a finite-mode approximation. We linearise around the steady state, which decouples the problem into subsystems.

In Section 3, we reproduce the “stable disc theorem” from [12] in this new setting. This theorem states that for classes whose mode numbers  $\mathbf{a}$  satisfy  $|\mathbf{a}| > |\mathbf{p}|$  the spectrum is stable. Thus most class subsystems do not contribute unstable modes to the spectrum of the full operator. Then our “unstable disc theorem” is proved which states that if exactly one mode number of a given class is inside the unstable disc then for sufficiently large  $N$  there is a positive real eigenvalue. In Theorem 3.4 we show that with certain additional assumptions this real eigenvalue is bounded away from zero when  $N \rightarrow \infty$ .

Section 4 establishes when the conditions for the lower bound established in Section 3 are met in the context of Zeitlin’s truncation. This provides the main theorem demonstrating instability of the stationary solution (1.2) for many choices of  $\mathbf{p}$ . Zeitlin’s scheme requires some care when proving results for both stable and unstable classes. Specifically it is not clear that the intersections between our classes and the disc  $|\mathbf{a}| < |\mathbf{p}|$  behave in the way we expect. We show that for most choices of  $\mathbf{p}$ , there is an appropriate truncation size  $N$  to control the results of the Zeitlin truncation so that Theorem 3.4 can be applied.

Section 5 provides some numerical results. The numerical efficiency and accuracy of Zeitlin’s truncation is compared favourably to a Galerkin-type truncation. A connection is made between the nature of the subsystems and the number and type of non-imaginary

eigenvalues. A discussion of the number of non-imaginary eigenvalues is included, and the accuracy of our calculated lower bound is assessed. A brief section on the pure imaginary spectrum of our finite mode systems is included, replicating the results in [11] via a very different method. We can show that the pure imaginary spectrum of our finite dimensional approximation approaches the essential spectrum of the full system. As a result we can naturally define a density of eigenvalues in the essential spectrum.

## 2. VORTICITY EVOLUTION IN FOURIER SPACE, TRUNCATION, LINEARISATION

**2.1. Hamiltonian Formulation.** The stream function  $\Psi$  is defined through its relation to the fluid velocities by

$$(2.1) \quad u_1 = +\frac{\partial\Psi}{\partial x_2}, \quad u_2 = -\frac{\partial\Psi}{\partial x_1}.$$

The relationship between the stream function and the vorticity is

$$(2.2) \quad \Omega = -\nabla^2\Psi$$

and hence the PDE can be written as

$$(2.3) \quad \frac{\partial\Omega}{\partial t} = \frac{\partial\Omega}{\partial x_1} \frac{\partial\Psi}{\partial x_2} - \frac{\partial\Omega}{\partial x_2} \frac{\partial\Psi}{\partial x_1}.$$

For a fixed  $\mathbf{p} \in \mathbb{Z}^2$  and  $\Gamma \in \mathbb{R}$  we wish to analyse the fixed point  $\Omega^* = 2\Gamma \cos(\mathbf{p} \cdot \mathbf{x})$ . Expand  $\Omega$  into a Fourier series with coefficients  $\omega_{\mathbf{k}}(t) \in \mathbb{C}$  as  $\Omega(\mathbf{x}, t) = \sum_{\mathbf{k} \in \mathbb{Z}^2} \omega_{\mathbf{k}}(t) e^{i\mathbf{k} \cdot \mathbf{x}}$  and combine (2.2) and (2.3). Then the Fourier coefficients are governed by the ODEs

$$(2.4) \quad \dot{\omega}_{\mathbf{k}}(t) = \sum_{\mathbf{l} \in \mathbb{Z}^2 \setminus \{\mathbf{0}\}} \frac{\mathbf{k} \times \mathbf{l}}{|\mathbf{l}|^2} \omega_{-\mathbf{l}} \omega_{\mathbf{k}+\mathbf{l}}$$

(where  $\mathbf{x} \times \mathbf{y} = x_1 y_2 - x_2 y_1$  for  $\mathbf{x}, \mathbf{y} \in \mathbb{R}^2$ , and  $\dot{\omega}_{\mathbf{k}} := \frac{d}{dt}(\omega_{\mathbf{k}})$ ). The condition  $\omega_{\mathbf{k}} = \overline{\omega_{-\mathbf{k}}}$  is necessary for  $\Omega$  to be real.

Define the ‘ideal fluid’ Poisson Bracket in Fourier Space as

$$(2.5) \quad \{f, g\} = \sum_{\mathbf{k}, \mathbf{l}} \frac{\partial f}{\partial \omega_{\mathbf{k}}} \frac{\partial g}{\partial \omega_{\mathbf{l}}} (\mathbf{k} \times \mathbf{l}) \omega_{\mathbf{k}+\mathbf{l}}.$$

The corresponding infinite dimensional Poisson structure matrix is  $J_{\mathbf{k}, \mathbf{l}} = (\mathbf{k} \times \mathbf{l}) \omega_{\mathbf{k}+\mathbf{l}}$ . Then (2.4) is a non-canonical Hamiltonian system with corresponding Hamiltonian

$$(2.6) \quad H = \frac{1}{2} \sum_{\mathbf{k} \in \mathbb{Z}^2 \setminus \{\mathbf{0}\}} \frac{\omega_{+\mathbf{k}} \omega_{-\mathbf{k}}}{|\mathbf{k}|^2} = \frac{1}{2} \sum_{\mathbf{k} \in \mathbb{Z}^2 \setminus \{\mathbf{0}\}} \frac{|\omega_{+\mathbf{k}}|^2}{|\mathbf{k}|^2}.$$

The Hamiltonian is obtained from the Kinetic energy

$$H = \frac{1}{2} \int \|\mathbf{u}\|^2 d\mathbf{x} = -\frac{1}{2} \int \Omega \Psi d\mathbf{x},$$

see e.g. [15].

**2.2. Zeitlin's Truncation.** We now truncate to a finite mode approximation and study the spectrum of the equilibrium corresponding to  $\Omega^*$ . Define the domain for our truncated Fourier modes

$$(2.7) \quad \mathcal{D} = [-N, N]^2 \cap \mathbb{Z}^2.$$

That is, we restrict to Fourier modes with mode numbers  $\mathbf{k} = (k_1, k_2)^T$  such that  $-N \leq k_1, k_2 \leq N$ . Introduce the notation  $\widehat{\mathbf{k}}$  to indicate taking  $\mathbf{k} \bmod 2N+1$  such that  $\widehat{\mathbf{k}} \in \mathcal{D}$ . For instance, if  $\mathbf{k} = (+N+1, +N+1)^T$  then  $\widehat{\mathbf{k}} = (-N, -N)^T$ , and if  $\mathbf{k} = (-N-1, -N-1)^T$  then  $\widehat{\mathbf{k}} = (+N, +N)^T$ .

Zeitlin [21] (see also [16]) gave the following Poisson bracket on this domain:

$$(2.8) \quad \{f, g\} = \sum_{\mathbf{k}, \mathbf{l} \in \mathcal{D}} \frac{\sin(\varepsilon \mathbf{k} \times \mathbf{l})}{\varepsilon} \frac{\partial f}{\partial \omega_{\mathbf{k}}} \frac{\partial g}{\partial \omega_{\mathbf{l}}} \omega_{\mathbf{k}+\mathbf{l} \bmod 2N+1},$$

$$(2.9) \quad J_{\mathbf{k}, \mathbf{l}} = \frac{1}{\varepsilon} \sin(\varepsilon \mathbf{k} \times \mathbf{l}) \omega_{\mathbf{k}+\mathbf{l} \bmod 2N+1}$$

where  $\mathbf{k}, \mathbf{l} \in \mathcal{D}$ , and  $\varepsilon = \frac{2\pi}{2N+1}$ . The corresponding truncation of (2.6) is the Hamiltonian

$$(2.10) \quad H = \frac{1}{2} \sum_{\mathbf{k} \in \mathcal{D} \setminus \{\mathbf{0}\}} \frac{\omega_{+\mathbf{k}} \omega_{-\mathbf{k}}}{|\mathbf{k}|^2},$$

where only the domain of summation has changed.

A simple Galerkin-style truncation (as described in [17] for example) truncates to a circular/spherical domain and sets all other Fourier coefficients to zero. Some advantages of Zeitlin's truncation over this method include (see [22]):

- The Lie algebra corresponds to  $su(N)$ ; as  $N \rightarrow \infty$  this tends to  $\text{sdiff}\mathbb{T}^2$ ;
- The corresponding bracket is indeed a Poisson bracket, unlike the Galerkin truncation where the bracket loses the Jacobi property at finite values of  $N$ ;
- There are  $2N+1$  Casimirs (conserved quantities).

For details of the construction and a description of the Casimirs see Zeitlin [21, 22].

For a fixed  $\mathbf{p} \in \mathcal{D} \setminus \{\mathbf{0}\}$  the equilibrium point of the PDE  $\Omega^* = 2\Gamma \cos(\mathbf{p} \cdot \mathbf{x})$  is an equilibrium point of the truncated ODE given by

$$(2.11) \quad \omega_{\mathbf{l}}^* = \begin{cases} \Gamma & \text{if } \mathbf{l} = \pm \mathbf{p} \\ 0 & \text{otherwise.} \end{cases}$$

We consider  $\Gamma \in \mathbb{R}$ ; the more general case  $\Gamma \in \mathbb{C}$  is treated in Li [12].

As the original problem has symmetries  $x \leftrightarrow -x$ ,  $y \leftrightarrow -y$ , and  $x \leftrightarrow y$ , we need only consider  $\mathbf{p} = (p_1, p_2)^T$  with  $p_1 \geq p_2 \geq 0$  and  $p_1 > 0$ .

The gradient of  $H$  is

$$(2.12) \quad (\nabla H)_{\mathbf{k}} = \begin{cases} \frac{\omega_{-\mathbf{k}}}{|\mathbf{k}|^2} & \text{if } \mathbf{k} \neq \mathbf{0} \\ 0 & \text{otherwise} \end{cases}.$$

The vector field can be written as

$$(2.13) \quad \dot{\omega}_{\mathbf{k}} = (J \nabla H)_{\mathbf{k}} = \sum_{\mathbf{l} \in \mathcal{D}} J_{\mathbf{k}, \mathbf{l}} \nabla H_{\mathbf{l}}$$

$$(2.14) \quad = \frac{1}{\varepsilon} \sum_{\mathbf{l} \in \mathcal{D}} \sin(\varepsilon \mathbf{k} \times \mathbf{l}) \omega_{\widehat{\mathbf{k}+\mathbf{l}}} \frac{\omega_{-\mathbf{l}}}{|\mathbf{l}|^2}.$$

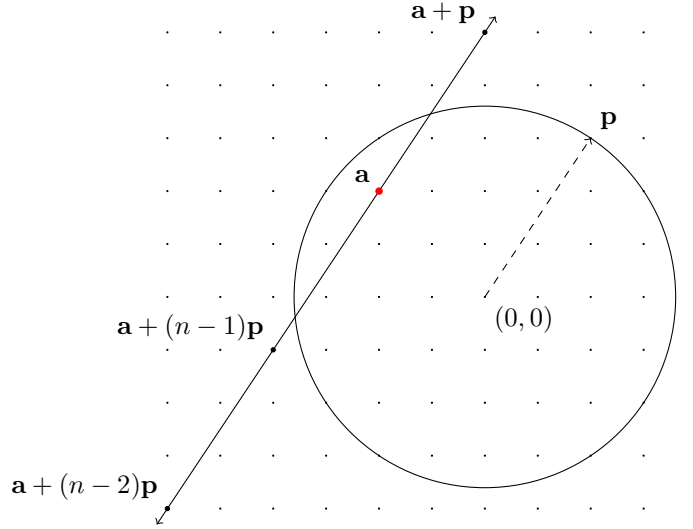


FIGURE 2.1. The differential equations governing the set of Fourier Coefficients decouple into ‘classes’ when linearised. Given a point  $\mathbf{a} \in \mathbb{Z}^2$ ,  $\dot{\omega}_{\mathbf{a}}$  depends only on  $\omega_{\mathbf{a}+\mathbf{p}}$  and  $\omega_{\mathbf{a}-\mathbf{p}}$ . Extending this ideas we get a subset of coefficients that only depend on each other, *the class led by  $\mathbf{a}$* . These coefficients all lie in a straight line with direction  $\mathbf{p}$ . The line shown here has  $|\mathbf{a}| < |\mathbf{p}|$ , which exactly corresponds to  $\rho_{\mathbf{a}} = \rho_0 < 0$ .

Thus the Jacobian of the Hamiltonian vector field is

$$(2.15) \quad D(J\nabla H)_{\mathbf{a},\mathbf{b}} = \begin{cases} 0 & \text{if } \mathbf{a} = \mathbf{b} \text{ or } \mathbf{b} = \mathbf{0} \\ \frac{1}{\varepsilon} \left( \frac{1}{|\mathbf{b}|^2} \sin(\varepsilon \mathbf{b} \times \mathbf{a}) + \frac{1}{|\widehat{(\mathbf{b}-\mathbf{a})}|^2} \sin(\varepsilon \mathbf{a} \times \widehat{(\mathbf{b}-\mathbf{a})}) \right) \omega_{\widehat{(\mathbf{a}-\mathbf{b})}}. \end{cases}$$

Evaluating this at the equilibrium (2.11) gives the linearised system about the equilibrium in Fourier space

$$(2.16) \quad \begin{aligned} \dot{\omega}_{\mathbf{k}} = & \frac{\Gamma}{2\varepsilon} \left( \frac{1}{|\widehat{(\mathbf{k}-\mathbf{p})}|^2} \sin(\varepsilon \widehat{(\mathbf{k}-\mathbf{p})} \times \mathbf{k}) + \frac{1}{|\mathbf{p}|^2} \sin(\varepsilon \mathbf{p} \times \mathbf{k}) \right) \omega_{\widehat{(\mathbf{k}-\mathbf{p})}} \\ & + \frac{\Gamma}{2\varepsilon} \left( \frac{1}{|\widehat{(\mathbf{k}+\mathbf{p})}|^2} \sin(\varepsilon \widehat{(\mathbf{k}+\mathbf{p})} \times \mathbf{k}) + \frac{1}{|\mathbf{p}|^2} \sin(\varepsilon \mathbf{k} \times \mathbf{p}) \right) \omega_{\widehat{(\mathbf{k}+\mathbf{p})}}. \end{aligned}$$

**2.3. Decoupling into Classes.** The key observation is that  $\dot{\omega}_{\mathbf{k}}$  depends only  $\omega_{\mathbf{k}\pm\mathbf{p}}$ . Thus the linearised system can be block-diagonalised. This block-diagonalisation is analogous to the construction in Li [12]. Following Li we call the individual blocks classes, which leads to the following definition:

**Definition 2.1** (Classes). For some  $\mathbf{a} \in \mathcal{D}$  (and  $\mathbf{p}$  fixed by the choice of equilibrium), the class  $\Sigma_{\mathbf{a}} \subset \mathcal{D}$  is defined by

$$(2.17) \quad \Sigma_{\mathbf{a}} = \{\widehat{\mathbf{a} + k\mathbf{p}} \in \mathcal{D} \mid k \in \mathbb{Z}\}.$$

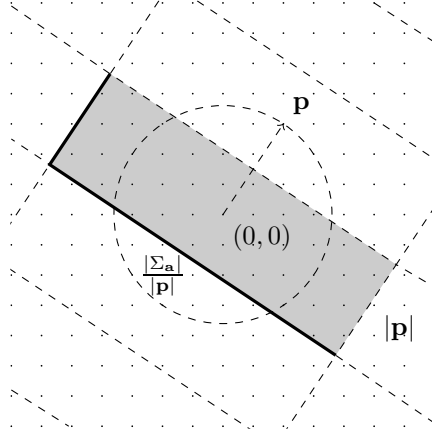


FIGURE 2.2. A canonical way of selecting values for  $\mathbf{a}$ . We choose values of  $\mathbf{a}$  in the shaded grey rectangle excluding the dashed boundaries. For typical values of  $\mathbf{p}$  this choice of  $\mathbf{a}$  is unique and all classes have a representative  $\mathbf{a}$ . This definition has the advantage that if  $\mathbf{a} \notin D_{\mathbf{p}}$ , then  $\mathbf{a} + \mathbf{p} \notin D_{\mathbf{p}}$  and  $\mathbf{a} - \mathbf{p} \notin D_{\mathbf{p}}$ . There is exactly one point from each class in every dashed rectangle. Note that there are some values of  $\mathbf{p}$  and choices of  $N$  where this construction is not possible; see Section 4.

Figure 2.1 illustrates this idea. Note that the classes ‘wrap around’ the Fourier mode domain  $\mathcal{D}$ . As  $\mathcal{D}$  is finite, there is some minimal  $n \in \mathbb{N}^+$  such that  $\widehat{\mathbf{a} + n\mathbf{p}} = \widehat{\mathbf{a}}$ , and so  $|\Sigma_{\mathbf{a}}| = n$  is finite. Li [12] makes the analogous definition for the non-truncated system. In that paper, the classes are infinitely large, and there are infinitely many classes. In our definition, there are finitely many classes of finite size, which depend on the truncation size  $N$ . Write  $\mathbf{p} = (p_1, p_2)^T$ , and  $\kappa = \gcd(p_1, p_2)$ . Then the number of points in  $\Sigma_{\mathbf{a}}$  is

$$(2.18) \quad |\Sigma_{\mathbf{a}}| = \frac{2N + 1}{\gcd(2N + 1, \kappa)}.$$

Note this does not depend on  $\mathbf{a}$ , and is odd for all choices of  $N$  and  $\mathbf{p}$ . We use this fact many times later. For  $\gcd(p_1, p_2) = 1$ ,  $|\Sigma_{\mathbf{a}}| = 2N + 1$ .

We can pick a ‘canonical’ choice for  $\mathbf{a}$  by restricting  $\mathbf{a}$  to be in a  $|\mathbf{p}|$  by  $\frac{|\Sigma_{\mathbf{a}}|}{|\mathbf{p}|}$  rectangle centred around  $\mathbf{0}$  and rotated so the sides of length  $|\mathbf{p}|$  are parallel to  $\mathbf{p}$ . This is illustrated in Figure 2.2. This choice is not possible for all values of  $\mathbf{p}$  and  $N$ . In particular, it will not work if  $\kappa > 1$ . See Section 4 and 4.1 for details.

Fixing  $\mathbf{p}$  and a canonical  $\mathbf{a}$  we now restrict our attention to the associated subsystem  $\Sigma_{\mathbf{a}}$ . Introduce new notation

$$(2.19) \quad \omega_k = \omega_{\widehat{\mathbf{a} + k\mathbf{p}}}, \quad \rho_k = \frac{1}{|\mathbf{p}|^2} - \frac{1}{|\widehat{\mathbf{a} + k\mathbf{p}}|^2} \quad \text{for } k = 0, 1, 2, \dots, n - 1$$

$$(2.20) \quad \alpha = \frac{\Gamma \sin(\varepsilon \widehat{(\mathbf{a} + k\mathbf{p})} \times \mathbf{p})}{\varepsilon} \in \mathbb{R}.$$

The value of the coefficient  $\rho_k$  is related to the distance of the lattice point  $\widehat{a + kp}$  from the boundary of the disc of radius  $|\mathbf{p}|$ , where negative values of  $\rho_k$  correspond to lattice points inside the disc. Note that  $\alpha$  does not depend on  $k$ . Also note that

$$(2.21) \quad \lim_{N \rightarrow \infty} \alpha = \lim_{\varepsilon \rightarrow 0} \alpha = \Gamma \mathbf{a} \times \mathbf{p}.$$

Noting that  $\sin(\varepsilon(\widehat{\mathbf{k} + \mathbf{p}}) \times \mathbf{k}) = \sin(\varepsilon \mathbf{p} \times \mathbf{k})$  and rewriting (2.16) with the new notation gives a compact form of the linear system

$$(2.22) \quad \dot{\omega}_k = \alpha(\rho_{k+1}\omega_{k+1} - \rho_{k-1}\omega_{k-1}).$$

If we write  $\boldsymbol{\omega} = (\omega_0, \omega_1, \dots, \omega_{n-1})^T$ , then  $\dot{\boldsymbol{\omega}} = \alpha A \boldsymbol{\omega}$  where

$$(2.23) \quad A = \begin{pmatrix} 0 & +\rho_1 & 0 & 0 & \cdots & 0 & -\rho_{n-1} \\ -\rho_0 & 0 & +\rho_2 & 0 & \cdots & 0 & 0 \\ 0 & -\rho_1 & 0 & +\rho_3 & \cdots & 0 & 0 \\ 0 & 0 & -\rho_2 & 0 & \cdots & 0 & 0 \\ \vdots & \vdots & \vdots & \vdots & \ddots & \vdots & \vdots \\ 0 & 0 & 0 & 0 & \cdots & 0 & +\rho_{n-1} \\ +\rho_0 & 0 & 0 & 0 & \cdots & -\rho_{n-2} & 0 \end{pmatrix}.$$

If  $\mathbf{a} = \mathbf{0}$  or  $\mathbf{a}$  is parallel to  $\mathbf{p}$ ,  $\alpha = 0$ . Thus the associated class only contributes zero eigenvalues and will not contribute to the linear instability of the system. We can thus ignore the classes with  $\alpha = 0$ .

Note that

$$\frac{1}{|\mathbf{p}|} - \frac{1}{|\mathbf{a} + k\mathbf{p}|^2} = \frac{1}{|\mathbf{p}|} - \frac{1}{|-\mathbf{a} - k\mathbf{p}|^2}.$$

Thus the values of  $\rho_k$  in the class led by  $\mathbf{a}$  are equal to the values of  $\rho_{-k}$  in the class led by  $-\mathbf{a}$ . Thus the corresponding matrix  $A$  for the class  $-\mathbf{a}$  is the same as the matrix  $A$  for the class  $\mathbf{a}$  up to a reflection across the anti-diagonal. By reordering  $\boldsymbol{\omega}$  as  $\boldsymbol{\omega} = (\omega_0, \omega_{-1}, \dots, \omega_{-n+1})^T$  it is clear that the class led by  $\mathbf{a}$  and the class led by  $-\mathbf{a}$  have the same dynamics and the same spectrum. Thus the reality condition  $\omega_k = \overline{\omega_{-k}}$  is preserved and the stability is the same.

Compare the system from (2.22) and (2.23) to the corresponding Galerkin truncation, truncating to (say) the Fourier modes between  $\omega_{-k}$  and  $\omega_j$

$$(2.24) \quad B = \begin{pmatrix} 0 & +\rho_{-k+1} & 0 & 0 & \cdots & 0 & 0 \\ -\rho_{-k} & 0 & +\rho_{-k+2} & 0 & \cdots & 0 & 0 \\ 0 & -\rho_{-k+1} & 0 & +\rho_{-k+3} & \cdots & 0 & 0 \\ 0 & 0 & -\rho_{-k+2} & 0 & \cdots & 0 & 0 \\ \vdots & \vdots & \vdots & \vdots & \ddots & \vdots & \vdots \\ 0 & 0 & 0 & 0 & \cdots & 0 & +\rho_j \\ 0 & 0 & 0 & 0 & \cdots & -\rho_{j-1} & 0 \end{pmatrix}.$$

This does not require the modulo operation and so is tridiagonal.

The matrix  $A$  in (2.23) can be written as  $A = JS$  where

$$(2.25) \quad J = \begin{pmatrix} 0 & +1 & 0 & \cdots & 0 & -1 \\ -1 & 0 & +1 & \cdots & 0 & 0 \\ 0 & -1 & 0 & \cdots & 0 & 0 \\ \vdots & \vdots & \vdots & \ddots & \vdots & \vdots \\ 0 & 0 & 0 & \cdots & 0 & +1 \\ +1 & 0 & 0 & \cdots & -1 & 0 \end{pmatrix}, \quad S = \begin{pmatrix} \rho_0 & 0 & 0 & \cdots & 0 \\ 0 & \rho_1 & 0 & \cdots & 0 \\ 0 & 0 & \rho_3 & \cdots & 0 \\ \vdots & \vdots & \vdots & \ddots & \vdots \\ 0 & 0 & 0 & \cdots & \rho_{n-1} \end{pmatrix}.$$

As  $J$  is skew-symmetric (and circulant) and  $S$  is symmetric, this is a (non-canonical) Hamiltonian system.<sup>1</sup> From this it follows that if  $\lambda$  is an eigenvalue of  $A$  then  $-\lambda$ ,  $\bar{\lambda}$  and  $-\bar{\lambda}$  are also eigenvalues. Note that  $\det(J) = 0$  as  $J$  has odd size, and therefore  $J$  is not symplectic with a one-dimensional kernel.<sup>2</sup>

We now focus on the behaviour of the eigenvalues of  $A$  as a function of the  $\rho_k$  values. Note that there is a symmetry in  $\mathbf{a}$ . For every class  $\Sigma_{\mathbf{a}}$ , the class  $\Sigma_{-\mathbf{a}}$  generates the same set of eigenvalues. It is worth noting that  $\alpha(-\mathbf{a}) = \frac{\Gamma \sin(-\varepsilon \mathbf{a} \times \mathbf{p})}{\varepsilon} = -\alpha(\mathbf{a})$ , but as all eigenvalues occur in  $\pm$  pairs, this does not affect the spectrum. Thus for the full system rather than a particular class all eigenvalues occur with multiplicity a multiple of 2.

**Definition 2.2** (The Unstable Disc). Introduce the disc  $D_{\mathbf{p}}$

$$(2.26) \quad D_{\mathbf{p}} = \{\mathbf{x} \in \mathcal{D} \mid |\mathbf{x}| < |\mathbf{p}|\}.$$

This disc is shown in Figure 2.1. A simple but important observation is

**Lemma 2.3.** *A lattice point is inside the unstable disc if and only if the corresponding  $\rho$  is negative:*

$$(2.27) \quad \widehat{\mathbf{a} + k\mathbf{p}} \in D_{\mathbf{p}} \iff \rho_k < 0.$$

*Proof.* This is true as  $\rho_k < 0$  if and only if  $|\mathbf{a} + k\mathbf{p}| < |\mathbf{p}|$  from (2.19), which is exactly the condition that  $\widehat{\mathbf{a} + k\mathbf{p}} \in D_{\mathbf{p}}$ .  $\square$   $\square$

This is illustrated in Figure 2.1. The point  $\mathbf{a}$  inside the disc corresponds to  $\rho_0 < 0$  and the other points correspond to  $\rho_k > 0$ . Also note that

$$\widehat{\mathbf{a} + k\mathbf{p}} \in \partial D_{\mathbf{p}} \iff \rho_k = 0.$$

### 3. STABILITY AND INSTABILITY OF CLASSES

**3.1. Stable Classes.** The matrix  $A$  is similar to a skew-symmetric matrix by conjugation with

<sup>1</sup>As  $J$  is circulant one could write down its eigensystem explicitly by applying a discrete Fourier transform[9] and therefore find a set of canonical coordinates[19]. This will not be used in this paper, but is of interest.

<sup>2</sup>We can also write  $B = \tilde{J}S$  with  $S$  as above and  $\tilde{J}$  like  $J$  in (2.25) but without the top right and bottom left elements of  $J$ . Since  $|\Sigma_{\mathbf{a}}|$  is always odd, this again has one-dimensional kernel like  $J$ . So again we have a Hamiltonian system, however, with a different Hamiltonian structure. Only the structure  $J$  is derived from the truncated Poisson structure  $J_{k,1}$ , while  $\tilde{J}$  appears ‘by accident’ after linearising the non-canonical Galerkin truncation.

$$(3.1) \quad T = \begin{pmatrix} \sqrt{\rho_0} & 0 & 0 & \cdots & 0 \\ 0 & \sqrt{\rho_2} & 0 & \cdots & 0 \\ 0 & 0 & \sqrt{\rho_3} & \cdots & 0 \\ \vdots & \vdots & \vdots & \ddots & \vdots \\ 0 & 0 & 0 & \cdots & \sqrt{\rho_{n-1}} \end{pmatrix},$$

$$(3.2) \quad TAT^{-1} = \begin{pmatrix} 0 & +\sqrt{\rho_0\rho_1} & 0 & \cdots & -\sqrt{\rho_{n-1}\rho_0} \\ -\sqrt{\rho_0\rho_1} & 0 & +\sqrt{\rho_1\rho_2} & \cdots & 0 \\ 0 & -\sqrt{\rho_1\rho_2} & 0 & \cdots & 0 \\ \vdots & \vdots & \vdots & \ddots & \vdots \\ +\sqrt{\rho_{n-1}\rho_0} & 0 & 0 & \cdots & 0 \end{pmatrix}.$$

Here  $n = |\Sigma_{\mathbf{a}}|$ .

If  $\rho_k \geq 0$  for all  $k$ , this transformation is real and thus  $A$  is similar to a real skew-symmetric matrix. Thus all eigenvalues are purely imaginary and  $A$  can be diagonalised and so the class is linearly stable. By (2.27) this condition is true exactly if

$$(3.3) \quad \Sigma_{\mathbf{a}} \cap D_{\mathbf{p}} = \emptyset.$$

This is the finite-dimensional analogue of Li's *Unstable Disc Theorem* (Theorem III.1) in [12], though the method of proof used in that paper is naturally very different. A discussion of the details such as choice of  $\mathbf{p}$  and  $N$  required for (3.3) to hold follows in Section 4. Because of this result, only classes  $\Sigma_{\mathbf{a}}$  with  $\mathbf{a} \in D_{\mathbf{p}}$  can contribute linear instability. Also  $\mathbf{a} = \mathbf{0}$  implies  $\alpha = 0$  and so this class cannot contribute linear instability.

**3.2. Unstable Classes.** For classes with  $\mathbf{a} \in D_{\mathbf{p}}$ , there are three possibilities to consider:

- i) There is exactly one intersection between the class and the disc (ie,  $\Sigma_{\mathbf{a}} \cap D_{\mathbf{p}} = \{\mathbf{a}\}$ ). This can only occur when  $\mathbf{a}$  is chosen to be in the shaded area indicated in Figure 3.1.
- ii) There are exactly two consecutive intersections between the class and the disc (ie,  $\Sigma_{\mathbf{a}} \cap D_{\mathbf{p}} = \{\mathbf{a}, \mathbf{a} + \mathbf{p}\}$  or  $\Sigma_{\mathbf{a}} \cap D_{\mathbf{p}} = \{\mathbf{a}, \mathbf{a} - \mathbf{p}\}$ ). This occur when  $\mathbf{a} \in D_{\mathbf{p}}$  is chosen outside the shaded area indicated in Figure 3.1.
- iii) There are at least two non-consecutive intersections between the class and the disc (ie,  $\mathbf{a} \in \Sigma_{\mathbf{a}} \cap D_{\mathbf{p}}$  and  $\widehat{\mathbf{a} + k\mathbf{p}} \in \Sigma_{\mathbf{a}} \cap D_{\mathbf{p}}$  for some  $k \neq -1, 0, 1$ ).

Note that points on the boundary are treated as being outside the disc. Also note that it is not possible for three consecutive lattice points in a class to be in the unstable disc. If  $\mathbf{a}$ ,  $\mathbf{a} - \mathbf{p}$  and  $\mathbf{a} + \mathbf{p}$  were all in  $\overline{D_{\mathbf{p}}}$ , they would lie along a diameter as  $\overline{D_{\mathbf{p}}}$  has diameter  $2|\mathbf{p}|$  and the distance from  $\mathbf{a} - \mathbf{p}$  to  $\mathbf{a} + \mathbf{p}$  is  $2|\mathbf{p}|$ . Therefore  $\mathbf{a} = (0, 0)$  and  $\mathbf{a} \pm \mathbf{p} \in \partial\overline{D_{\mathbf{p}}}$ . This is the only possibility to have three consecutive lattice point in  $\overline{D_{\mathbf{p}}}$ , and hence  $D_{\mathbf{p}}$  can at most contain two consecutive lattice points. Figure 2.1 makes this idea clear.

From our numerical and analytical results we can categorise the spectrum of the class in these three cases:

- i) The spectrum has a single pair of real eigenvalues and all other eigenvalues on the imaginary axis. This is proved in Theorem 3.1.
- ii) The spectrum typically corresponds to a quartet of complex eigenvalues  $\pm\alpha \pm \beta i$ , and all other eigenvalues on the imaginary axis. It can also correspond to two pairs of real eigenvalues, though this is less common.

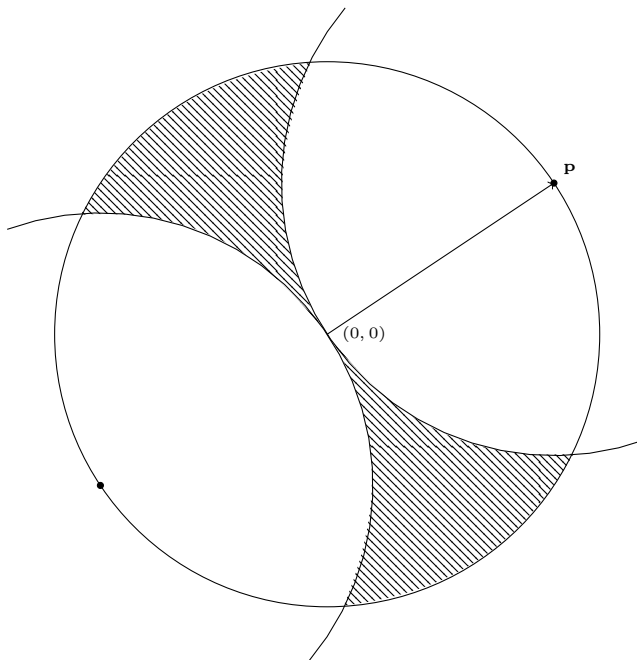


FIGURE 3.1. If  $\mathbf{a}$  is in the shaded region,  $\rho_0 < 0$  and  $\rho_1, \rho_{n-1} > 0$ . For case (i) to occur this must be true. The corresponding spectrum has a pair of real non-zero eigenvalues by Theorem 3.1. Note that any  $\mathbf{a}$  in the shaded region is a canonical choice of  $\mathbf{a}$  (cf. Figure 2.2). If  $\mathbf{a}$  is outside the shaded area but still inside the disc  $D_{\mathbf{p}}$  (case (ii)), this corresponds to either a complex quadruplet of eigenvalues or two pairs of real eigenvalues (more commonly the former). The large circle has centre  $(0, 0)$  and radius  $|\mathbf{p}|$ . The two large arcs have centres  $\pm\mathbf{p}$  and radius  $|\mathbf{p}|$ .

- iii) This corresponds to the class ‘wrapping around’ the truncated domain of lattice points and intersecting the disc again; see 4.1. The spectrum is a combination of case (i) and case (ii) according to how successive intersections with the disc occur.

This last case is atypical and does not occur with a Galerkin truncation. Usually this case can be avoided by a proper choice of  $N$ , however when both entries of  $\mathbf{p}$  are even, it cannot be avoided. This is discussed in detail in Section 4, particularly Lemma 4.1.

All our numerical evidence is consistent with the result in [11] that the number of eigenvalues with non-zero real part is  $\leq 2|D_{\mathbf{p}}|$  (twice the number of interior lattice points in the unstable disc), and our observation is that this is the *exact* number of hyperbolic eigenvalues.

For case (i), Theorem 3.1 proves that this case always leads to non-zero real eigenvalues. For some  $\mathbf{p}$  and  $\mathbf{a}$  leading to case (i), Theorem 3.4 describes an explicit lower bound which is independent of the truncation size  $N$  for the real eigenvalues. It should be noted that our methods do not preclude the possibility that there are other eigenvalues with non-zero real part unaccounted for; we simply assert that there is at least one eigenvalue with

positive real part. This together with the results from [8], [11], [18], and [13] is sufficient to conclude nonlinear instability for the whole system.

For this next section, we consider a general set of parameters  $(a_0, a_1, \dots, a_{n-1})$  instead of  $\rho_k$ . Introduce a tridiagonal matrix

$$(3.4) \quad T_\alpha^\beta = \begin{pmatrix} 0 & a_{\alpha+1} & 0 & 0 & \cdots & 0 & 0 \\ -a_\alpha & 0 & a_{\alpha+2} & 0 & \cdots & 0 & 0 \\ 0 & -a_{\alpha+1} & 0 & a_{\alpha+3} & \cdots & 0 & 0 \\ 0 & 0 & -a_{\alpha+2} & 0 & \cdots & 0 & 0 \\ 0 & 0 & 0 & -a_{\alpha+3} & \cdots & 0 & 0 \\ \vdots & \vdots & \vdots & \vdots & \ddots & \vdots & \vdots \\ 0 & 0 & 0 & 0 & \cdots & 0 & a_\beta \\ 0 & 0 & 0 & 0 & \cdots & -a_{\beta-1} & 0 \end{pmatrix},$$

and its characteristic polynomial

$$(3.5) \quad \mathcal{T}_\alpha^\beta(x) = \det(xI - T_\alpha^\beta)$$

for some integers  $0 \leq \alpha < \beta \leq n-1$ . Then  $\mathcal{T}_\alpha^\beta(x)$  can be recursively defined by expansion from top left to bottom right

$$(3.6) \quad \begin{aligned} \mathcal{T}_\alpha^\alpha(x) &= 1, & \mathcal{T}_\alpha^{\alpha+1}(x) &= x^2 + a_{\alpha+1}a_\alpha, \\ \mathcal{T}_\alpha^\beta(x) &= x\mathcal{T}_\alpha^{\beta-1}(x) + a_\beta a_{\beta-1} \mathcal{T}_\alpha^{\beta-2}(x). \end{aligned}$$

or by expansion from bottom right to top left

$$(3.7) \quad \begin{aligned} \mathcal{T}_\beta^\beta(x) &= 1, & \mathcal{T}_{\beta-1}^\beta(x) &= x^2 + a_{\beta-1}a_\beta, \\ \mathcal{T}_\alpha^\beta(x) &= x\mathcal{T}_{\alpha+1}^\beta(x) + a_\alpha a_{\alpha+1} \mathcal{T}_{\alpha+2}^\beta(x). \end{aligned}$$

Note that

$$(3.8) \quad a_k > 0 \text{ for all } \alpha \leq k \leq \beta \implies \mathcal{T}_\alpha^\beta(x) > 0 \text{ for all } x > 0.$$

This can be seen by the recursive definitions; all terms are positive. <sup>3</sup>

The following is also useful:

$$(3.9) \quad \mathcal{T}_\alpha^\beta(0) = \begin{cases} \prod_{k=\alpha}^{\beta} a_k & \text{if } \beta - \alpha \text{ is odd,} \\ 0 & \text{if } \beta - \alpha \text{ is even.} \end{cases}$$

$$(3.10) \quad \left. \frac{d}{dx} \mathcal{T}_\alpha^\beta(x) \right|_{x=0} = \begin{cases} 0 & \text{if } \beta - \alpha \text{ is odd,} \\ \sum_{k=0}^{\frac{\beta-\alpha}{2}} \left( \prod_{j=\alpha; j \neq \alpha+2k}^{\beta} a_j \right) & \text{if } \beta - \alpha \text{ is even.} \end{cases}$$

These can be proved by simple induction arguments.

---

<sup>3</sup>Note that the (3.6) and (3.7) satisfy the condition for Favard's theorem [7]. Thus the polynomials  $\mathcal{T}(x; a_1, \dots, a_j)$  are orthogonal for  $j = 1, 2, 3, \dots$  with respect to an inner product with some weight function (see [20]). However, as the  $a_k$  terms may be negative this weight function will not always be positive. This will not be used here, but may be useful in future work for describing the imaginary part of the spectrum.

Introduce similar notation for (2.23)

$$(3.11) \quad A = \begin{pmatrix} 0 & +a_1 & 0 & 0 & \cdots & 0 & -a_{n-1} \\ -a_0 & 0 & +a_2 & 0 & \cdots & 0 & 0 \\ 0 & -a_1 & 0 & +a_3 & \cdots & 0 & 0 \\ 0 & 0 & -a_2 & 0 & \cdots & 0 & 0 \\ \vdots & \vdots & \vdots & \vdots & \ddots & \vdots & \vdots \\ 0 & 0 & 0 & 0 & \cdots & 0 & +a_{n-1} \\ +a_0 & 0 & 0 & 0 & \cdots & -a_{n-2} & 0 \end{pmatrix},$$

with the characteristic polynomial

$$(3.12) \quad \mathcal{A}(x) = \det(xI - A).$$

Then, if  $n$  is odd,

$$(3.13) \quad \begin{aligned} \mathcal{A}(x) &= x\mathcal{T}_0^{n-2}(x) + a_{n-1}a_{n-2}\mathcal{T}_0^{n-3}(x) + a_{n-1}a_0\mathcal{T}_1^{n-2}(x) \\ &= \mathcal{T}_0^{n-1}(x) + a_0a_{n-1}\mathcal{T}_1^{n-2}(x) \end{aligned}$$

This can be demonstrated by expanding by minors along the last row and column of  $xI - A$ . Recall that  $n$  is odd for the relevant problem ( $n = |\Sigma_{\mathbf{a}}|$  from equation (2.18)).

We first show that in case (i) there is some non-zero real eigenvalue. Because of the Hamiltonian nature of the system this means there is a plus/minus pair of eigenvalues and so there is linear instability. This is then extended to show that under certain conditions there is pair of real eigenvalues with an explicit lower bound independent of  $N$ .

**Theorem 3.1** (Real Eigenvalues in case (i)). *If  $\rho_0 < 0$ , and  $\rho_k \geq 0$  for all  $k = 1, 2, \dots, n-1$  and  $\rho_k = 0$  for at most one of  $k = 1, 2, \dots, n-1$ , then for sufficiently large  $N$ , (2.23) has a non-zero real eigenvalue.*

*Proof.* The characteristic polynomial  $\mathcal{A}$  for odd  $n$  has leading term  $x^n$  and constant term 0. By combining (3.13) and (3.10) (noting that  $n$  is odd, so  $n-1$  and  $n-3$  are even), the linear coefficient is given by

$$(3.14) \quad \begin{aligned} \left. \frac{d\mathcal{A}}{dx} \right|_{x=0} &= \left. \frac{d}{dx} \mathcal{T}_0^{n-1}(x) \right|_0 + a_0a_{n-1} \left. \mathcal{T}_1^{n-2}(x) \right|_0 \\ &= \sum_{k=0}^{\frac{n-1}{2}} \left( \prod_{j=0; j \neq 2k}^{n-1} a_j \right) + \sum_{k=0}^{\frac{n-3}{2}} \left( \prod_{j=1; j \neq 1+2k}^{n-2} a_j \right) \\ &= \sum_{k=0}^{n-1} \left( \prod_{j=0; j \neq k}^{n-1} a_j \right) \end{aligned}$$

$$(3.15) \quad = \left( \prod_{j=0}^{n-1} a_j \right) \left( \sum_{k=0}^{n-1} \frac{1}{a_k} \right).$$

Note that (3.15) is only valid for  $a_k \neq 0$  for all  $k$ , but (3.14) is always valid<sup>4</sup>. Now let  $a_k = \rho_k$ . First assume  $\rho_k > 0$  for all  $k \neq 0$ . As  $\rho_k \rightarrow \frac{1}{|\mathbf{p}|^2} > 0$  as  $|\mathbf{a} + k\mathbf{p}| \rightarrow \infty$  and the

<sup>4</sup>The expression in equation (3.14) is the so-called  $n-1^{\text{st}}$  elementary symmetric polynomial in the variables  $a_j$

size  $n$  of the classes grows linearly with  $N$ ,  $\sum_{j=0}^{n-1} \frac{1}{a_j} = \sum_{j=0}^{n-1} \frac{1}{\rho_j} > 0$  for sufficiently large  $N$  (where  $\rho_k = a_k$ ). However  $\prod_{j=0}^{n-1} a_j < 0$  as  $a_0 < 0$ ,  $a_j > 0$  for all  $j = 1, \dots, n-1$ , and hence the linear coefficient of the characteristic polynomial is less than zero.

If  $\rho_k = 0$  for exactly one  $k$ , then (3.14) consists of only one term,  $\prod_{j=0; j \neq k}^{n-1} \rho_j$ . This is less than zero as  $\rho_0 < 0$  and  $\rho_j > 0$  for all  $j \neq 0, k$ .

If  $\rho_k = 0$  for more than one value of  $k$ , then the linear term is zero and we cannot apply this argument.

As the constant term is zero, and the linear term is non-zero, then the lowest order non-zero coefficient of the polynomial is negative.

We now argue by contradiction. Assume all roots of the polynomial are imaginary (say  $i\omega_k$ ) or complex ( $\gamma_j + i\delta_j$ ) or zero. Then because eigenvalues occur in positive and negative pairs as well as conjugate pairs the polynomial has the form

(3.16)

$$\begin{aligned} \mathcal{A}(x) &= \\ & x^{n_1} \prod_{k=1}^{n_2} (x - i\omega_k)(x + i\omega_k) \prod_{j=1}^{n_3} [(x - \gamma_j - i\delta_j)(x - \gamma_j + i\delta_j)(x + \gamma_j - i\delta_j)(x + \gamma_j + i\delta_j)] \\ (3.17) \quad &= x^{n_1} \prod_{k=1}^{n_2} (x^2 + \omega_k^2) \prod_{j=1}^{n_3} (x^4 - 2x^2(\gamma_j^2 - \delta_j^2) + (\gamma_j^2 + \delta_j^2)^2). \end{aligned}$$

The lowest order non-zero coefficient (of  $x^{n_1}$ ) is  $\prod_{k=1}^{n_2} (\omega_k^2) \prod_{j=1}^{n_3} ((\gamma_j^2 + \delta_j^2)^2) > 0$ . Thus by contradiction there must be some real eigenvalue, which will occur in a plus and minus pair.  $\square$

Note that there is not yet a guarantee that the real eigenvalues will not be vanishingly small as  $N \rightarrow \infty$ . This is addressed by the following.

**Lemma 3.2** (Lower Bound for Real Eigenvalue). *If  $a_0 < 0$ , and  $a_k \geq 0$  for all  $k \neq 0$ , and  $a_0 + a_2 < 0$ , then*

$$(3.18) \quad \mathcal{A}(\sqrt{-a_1(a_0 + a_2)}) \leq 0.$$

*Proof.* By expanding (3.13) using (3.7),

$$\begin{aligned} \mathcal{A}(x) &= (x^3 + (a_0 a_1 + a_1 a_2)x) \mathcal{T}_3^{n-1}(x) \\ & \quad + (x^2 + a_0 a_1) a_2 a_3 \mathcal{T}_4^{n-1}(x) \\ (3.19) \quad & \quad + a_0 a_{n-1} \mathcal{T}_1^{n-2}(x). \end{aligned}$$

Thus

$$\begin{aligned} \mathcal{A}(\sqrt{-a_1(a_0 + a_2)}) &= -a_1 a_2^2 a_3 \mathcal{T}_4^{n-1}(\sqrt{-a_1(a_0 + a_2)}) \\ (3.20) \quad & \quad + a_0 a_{n-1} \mathcal{T}_1^{n-2}(\sqrt{-a_2(a_1 + a_3)}). \end{aligned}$$

As  $a_1, a_2, a_3, a_{n-1} \geq 0$ ,  $a_0 < 0$  and the  $\mathcal{T}$  terms are positive by (3.8) the result follows.  $\square$

We can also make a similar construction if  $a_0 < 0$ ,  $a_k \geq 0$  for all  $k \neq 0$  and  $a_0 + a_{n-2} < 0$ . In this case,

$$(3.21) \quad \mathcal{A}(\sqrt{-a_{n-1}(a_0 + a_{n-2})}) \leq 0.$$

**Lemma 3.3.** *Assuming the same conditions as Lemma 3.2, there exists some*

$$x^* \geq \sqrt{-a_1(a_0 + a_2)}$$

such that  $\mathcal{A}(x^*) = 0$ .

*Proof.* The leading order term of  $\mathcal{A}(x)$  is always  $x^n$  regardless of  $a_0, \dots, a_{n-1}$ , and  $\mathcal{A}(x)$  is real for real  $x$ . Thus  $\lim_{x \rightarrow \infty} \mathcal{A}(x) > 0$ . But by Lemma 3.2  $\mathcal{A}(\sqrt{-a_1(a_0 + a_2)}) \leq 0$ , and the result follows by the intermediate value theorem.  $\square$   $\square$

Note that it is possible that  $\sqrt{-a_1(a_0 + a_2)} = 0$ , and thus  $x^*$  may also equal 0.

We now turn our attention back to the context of our problem.

**Theorem 3.4** (Lower Bound for Real Eigenvalues in case (i)). *If  $\mathbf{a} \in D_{\mathbf{p}}$  and  $\widehat{\mathbf{a} + k\mathbf{p}} / \in D_{\mathbf{p}}$  for  $k = 1, 2, \dots, n-1$  and*

$$(3.22) \quad \lambda^\dagger = \sqrt{-\rho_1(\rho_0 + \rho_2)}$$

is real, there exists  $\lambda \geq \lambda^\dagger$  such that  $\lambda$  is an eigenvalue of (2.23).

Similarly if  $\lambda^\dagger = \sqrt{-\rho_{n-1}(\rho_0 + \rho_{n-2})}$  is real there exists  $\lambda \geq \lambda^\dagger$  such that  $\lambda$  is an eigenvalue of (2.23).

*Proof.* This follows from the previous two lemmas, letting  $\rho_i = a_i$  and making note of (2.27).  $\square$   $\square$

Section 4 clarifies under what conditions  $\lambda^\dagger$  is real, and Theorem 3.4 holds. For example, when  $\mathbf{p} = (1, 1)^T$  then  $\mathbf{a} = (0, 1)^T$  leads to a case (i) class, so Theorem 3.1 holds, but the reality conditions in Theorem 3.4 are not satisfied. It is also possible that  $\lambda^\dagger = 0$ , so the real eigenvalue could be zero, so we also require that  $\lambda^\dagger > 0$ . A sufficient condition on  $\mathbf{a}$  for this to hold is given in Lemma 4.2.

#### 4. INSTABILITY OF EQUILIBRIA

To prove instability of an equilibrium for a given  $\mathbf{p}$  we need to find at least one unstable class  $\Sigma_{\mathbf{a}}$ . A necessary condition for a lattice point  $\mathbf{a}$  to lead to an unstable class is to be inside the unstable disc. More precisely we desire a lattice point  $\mathbf{a}$  that leads to a class  $\Sigma_{\mathbf{a}}$  of case (i) as this is the simplest situation to deal with. Theorem 3.4 asserts that there is a real eigenvalue with an explicit lower bound under some certain conditions. The goal now is to determine for which  $\mathbf{p}$  there exists a lattice point  $\mathbf{a}$  such that the conditions of Theorem 3.4 are satisfied.

Although Zeitlin's truncation [21] preserves the geometric structure and the Casimirs of the original problem, it introduces a problem that is not present in [12]. This has already been mentioned in the classification of classes; it is the appearance of case (iii), in which a class intersects the unstable disc at non-consecutive points. This may occur because now we have periodic boundary conditions not only in physical space, but also in Fourier space. There are two distinct problems caused by this, as illustrated in Figure 4.1.

The lattice points of a class lie on parallel line segments with direction vector  $\mathbf{p}$  in the domain of Fourier modes. In general there is more than one such line segment in the domain. The first problem appears when the distance between these line segments is so

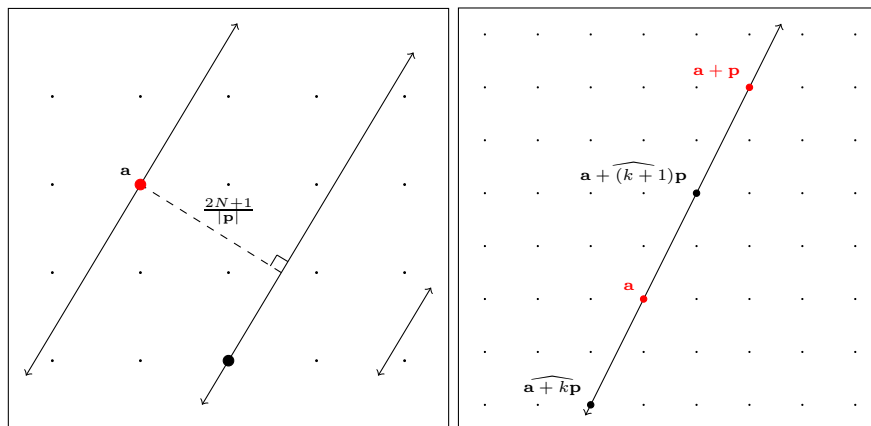


FIGURE 4.1. For fixed  $\mathbf{p}$  and  $\mathbf{a}$ , there are some concerns with the wrapping of the truncation and the way this affects the intersection  $\Sigma_{\mathbf{a}} \cap D_{\mathbf{p}}$ . These situations are discussed in Lemma 4.1.

*Left:* the shortest distance between  $\mathbf{a}$  and some non-consecutive  $\widehat{\mathbf{a} + k\mathbf{p}}$  is at least  $\frac{2N+1}{|\mathbf{p}|}$ . As we are interested in the limit  $N \rightarrow \infty$ , this distance can be made arbitrarily large, so that  $\frac{2N+1}{|\mathbf{p}|} > 2|\mathbf{p}|$ . This ensures that  $\mathbf{a}$  and  $\widehat{\mathbf{a} + k\mathbf{p}}$  cannot both be in the disc  $D_{\mathbf{p}}$ .

*Right:* The situation where there exists  $k \in \mathbb{R}$  such that  $\widehat{\mathbf{a} + k\mathbf{p}}$  lies on the line segment between  $\mathbf{a}$  and  $\mathbf{a} + \mathbf{p}$ . This causes problems for our values of  $\rho$ . For  $\widehat{\mathbf{a} + k\mathbf{p}}$  to lie at a lattice point on the line segment,  $\gcd(p_1, p_2) > 1$ . If  $\gcd(p_1, p_2)$  is odd, we can avoid this situation by choosing  $N$  per Equation (4.1); if  $p_1$  and  $p_2$  are both even this situation is unavoidable.

small that more than one line segment intersects the unstable disc. This can be fixed by making  $N$  sufficiently large. The second problem occurs when non-consecutive lattice points lie on the same line segment intersecting the unstable disc. If  $\gcd(p_1, p_2)$  is not even this can be fixed by choosing  $N$  per (4.1). Note that for our purposes,  $\gcd(p_1, 0) = p_1$  and  $\gcd(p_1, p_2) = \gcd(|p_1|, |p_2|)$ .

**Lemma 4.1.** *For all  $\mathbf{p} = (p_1, p_2)^T$  such that  $\kappa = \gcd(p_1, p_2)$  is not even, there exists a sequence of  $N$  which increases without bound such that for all choices of  $\mathbf{a}$  any two non-consecutive lattice points in  $\Sigma_{\mathbf{a}}$  cannot both be in the unstable disc.*

*Proof.* Let

$$(4.1) \quad N = \frac{(2A+1)\kappa - 1}{2}$$

for  $A \in \mathbb{N}$ . Thus  $2N+1 = (2A+1)\kappa$ . If  $\kappa$  is not even, then such an  $N$  is a positive integer and thus a valid grid size. Select as a lower bound  $A > \frac{2|\mathbf{p}|^2 - \kappa}{2\kappa}$  so that  $N > \frac{2|\mathbf{p}|^2 - 1}{2}$ .  $\mathbf{p}$  is fixed and finite so this lower bound is always finite. We can thus find an infinite sequence of  $N$  that increases without bound by letting  $A$  increase without bound.

If  $\mathbf{x} \in \Sigma_{\mathbf{a}}$  then  $\mathbf{x} = \widehat{\mathbf{a} + k\mathbf{p}}$  for some  $k \in \mathbb{N}$ . Thus  $\mathbf{x}$  lies on the line parallel to the vector  $\mathbf{p}$  that passes through the point  $\mathbf{a} + \Delta_{\mathbf{x}}(2N+1)$  for some  $\Delta_{\mathbf{x}} \in \mathbb{Z}^2$  (note that this point will be outside the domain  $\mathcal{D}$ ).

Similarly if  $\mathbf{y} \in \Sigma_{\mathbf{a}}$  then it lies on the line parallel to  $\mathbf{p}$  that passes through  $\mathbf{a} + \Delta_{\mathbf{y}}(2N+1)$  for some  $\Delta_{\mathbf{y}} \in \mathbb{Z}^2$ . Then the distance between these two lines is

$$(4.2) \quad d = \frac{|((\mathbf{a} + \Delta_{\mathbf{x}}(2N+1)) - (\mathbf{a} + \Delta_{\mathbf{y}}(2N+1))) \times \mathbf{p}|}{|\mathbf{p}|} = \frac{(2N+1)|(\Delta_{\mathbf{x}} - \Delta_{\mathbf{y}}) \times \mathbf{p}|}{|\mathbf{p}|}.$$

$(\Delta_{\mathbf{x}} - \Delta_{\mathbf{y}}) \times \mathbf{p} \in \mathbb{Z}^2$ , so  $d = 0$  or  $d \geq \frac{2N+1}{|\mathbf{p}|}$ . If  $d \geq \frac{2N+1}{|\mathbf{p}|}$ , this corresponds to  $\mathbf{x}$  and  $\mathbf{y}$  lying on different line segments, as in Figure 4.1. Thus the distance between two points on different line segments is at least  $\frac{2N+1}{|\mathbf{p}|} > 2|\mathbf{p}|$  for our choice of  $N$ .

If  $d = 0$ , then  $\mathbf{x}$  and  $\mathbf{y}$  must lie on the same line segment. Thus  $\mathbf{y}$  lies on the line parallel to  $\mathbf{p}$  passing through  $\mathbf{x}$ .

Write  $\mathbf{p} = \kappa\mathbf{q}$  so  $\mathbf{q} = (q_1, q_2)^T$  where  $\gcd(q_1, q_2) = 1$ . Then as  $\mathbf{x}, \mathbf{y} \in \mathbb{Z}^2$ ,  $\mathbf{y} = \mathbf{x} + k\mathbf{q}$  for some  $k \in \mathbb{Z}$ . But  $\mathbf{x}, \mathbf{y} \in \Sigma_{\mathbf{a}}$  so  $\mathbf{y} = \mathbf{x} + j\mathbf{p} + (2N+1)\Delta$  for some  $\Delta \in \mathbb{Z}^2$ .

Thus  $k\mathbf{q} = j\mathbf{p} + (2N+1)\Delta$ . So

$$k\mathbf{q} = j\kappa\mathbf{q} + (2N+1)\kappa\Delta = \kappa(j\mathbf{q} + (2N+1)\Delta).$$

Thus  $k\mathbf{q}$  is divisible by  $\kappa$ , but the elements of  $\mathbf{q}$  both be divided by  $\kappa$  by definition, so  $\kappa|k$ . Thus  $\mathbf{y} = \mathbf{x} + \kappa\beta\mathbf{q}$  for some  $\beta \in \mathbb{Z}$ , and so  $\mathbf{y} = \mathbf{x} + \beta\mathbf{p}$ . Then if  $|\mathbf{y} - \mathbf{x}| < 2|\mathbf{p}|$  (the necessary condition for  $\mathbf{x}, \mathbf{y}$  both in  $D_{\mathbf{p}}$ ) this implies  $\beta = 0$  or  $\beta = \pm 1$ , and the result follows.  $\square$

**Lemma 4.2.** *For all  $\mathbf{p} = (p_1, p_2)^T$  except  $(1, 0)^T, (1, 1)^T, (1, 2)^T$  (and permutations and sign changes thereof) such that  $\kappa = \gcd(p_1, p_2)$  is not even there exists a choice of  $\mathbf{a}$  such that the reality conditions of Theorem 3.4 are satisfied for an appropriate choice of  $N$ .*

*Proof.* For the bound given in Theorem 3.2 to be real, positive, and hence a valid bound, we require  $\rho_0 < 0$ ,  $\rho_k \geq 0$  for all  $k \neq 0$ , and  $\rho_0 + \rho_2 < 0$  (or  $\rho_0 + \rho_{n-2} < 0$ ).

If  $\rho_0 < 0$ ,  $\rho_1, \rho_{-1} > 0$ , then  $|\mathbf{a}| < |\mathbf{p}|$  and  $|\mathbf{a} \pm \mathbf{p}| > |\mathbf{p}|$ . This condition on  $\mathbf{a}$  is illustrated in Figure 3.1. By Lemma 4.1, we can find an unbounded sequence of choices of  $N$  such that for any  $k \neq 0, -1, +1$   $|\widehat{\mathbf{a} + k\mathbf{p}}| > |\mathbf{p}|$ , and so we only need to prove that  $|\mathbf{a} \pm \mathbf{p}| > |\mathbf{p}|$ .

As  $\lambda^\dagger = \sqrt{-\rho_1(\rho_0 + \rho_2)}$  (or equivalently  $\lambda^\dagger = \sqrt{-\rho_{-1}(\rho_0 + \rho_{-2})}$ ) is required to be real and non-zero, and  $\rho_{-1} > 0$ , then  $\rho_0 + \rho_2 < 0$  (equivalently  $\rho_0 + \rho_{-2} < 0$ ).

If  $|\mathbf{a}| < (\sqrt{3}-1)|\mathbf{p}|$ , then  $|\mathbf{a} \pm 2\mathbf{p}| \leq |\mathbf{a}| + 2|\mathbf{p}| < (\sqrt{3}+1)|\mathbf{p}|$ . So

$$(4.3) \quad \begin{aligned} \rho_0 + \rho_{\pm 2} &= \frac{1}{|\mathbf{p}|^2} - \frac{1}{|\mathbf{a}|^2} + \frac{1}{|\mathbf{p}|^2} - \frac{1}{|\mathbf{a} \pm 2\mathbf{p}|^2} \\ &< \frac{2}{|\mathbf{p}|^2} - \frac{1}{|(\sqrt{3}-1)\mathbf{p}|^2} - \frac{1}{|(\sqrt{3}+1)\mathbf{p}|^2} \\ &= 0. \end{aligned}$$

We thus need to show there exists some  $\mathbf{a}$  such that  $|\mathbf{a}| < (\sqrt{3}-1)|\mathbf{p}|$  and  $|\mathbf{a} \pm \mathbf{p}| > |\mathbf{p}|$ . These two conditions are illustrated in Figure 4.2 in the shaded region. Note that this is sufficient but not necessary for Theorem 3.4 to hold.

The idea now is to specify that  $\mathbf{a}$  is in the disc inscribed by the shaded region in Figure 4.2, which we call  $D_c$ . This disc is tangent to the circles with radii  $|\mathbf{p}|$  and centres  $\pm\mathbf{p}$  and

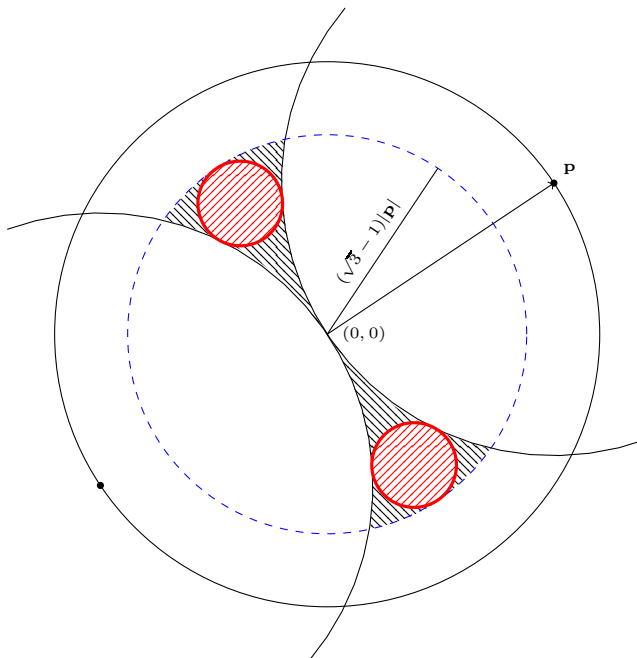


FIGURE 4.2. If  $\mathbf{a}$  is in the dashed blue circle, then  $\rho_0 + \rho_2 < 0$  and  $\rho_0 + \rho_{n-2} < 0$ . This circle has centre  $(0, 0)$  and radius  $(\sqrt{3} - 1)|\mathbf{p}|$ . The shaded region here shows the overlap of this condition and the condition illustrated in Figure 3.1. To show that there is at least one lattice point in the shaded regions we show the disc  $D_c$  inscribed in this region (indicated by the small red circles) has radius larger than  $1/\sqrt{2}$ .

the circle centred at the origin with radius  $(\sqrt{3} - 1)|\mathbf{p}|$ . It is a simple geometric exercise to show that such a circle has centre  $\pm \frac{1}{\sqrt{3}} \begin{pmatrix} -p_2 \\ p_1 \end{pmatrix}$  and radius  $(\frac{2}{\sqrt{3}} - 1)|\mathbf{p}|$ .

If  $\mathbf{a} \in D_c$ , it is outside the circle with centre  $-\mathbf{p}$  and radius  $|\mathbf{p}|$ . Thus  $\mathbf{a} + \mathbf{p}$  is outside  $D_{\mathbf{p}}$  and  $\rho_1 > 0$ . Similarly,  $\rho_{-1} > 0$ . As  $D_c$  is inside the disc with centre origin and radius  $(\frac{2}{\sqrt{3}} - 1)|\mathbf{p}|$  clearly  $\rho_0 < 0$  and by the above  $\rho_0 + \rho_{\pm 2} < 0$ . For appropriate choices of  $N$   $\rho_k \geq 0$  for all  $k \neq 0$  by Lemma 4. Then the conditions of Theorem 3.4 are satisfied and the resulting bound  $\lambda^\dagger$  is real and positive.

All that remains is to show that there exists an integer lattice point  $\mathbf{a} \in D_c$ . Any disc with a radius greater than  $\frac{1}{\sqrt{2}}$  must contain some integer lattice point (as it wholly contains a square of side length 1). Thus if

$$(4.4) \quad |\mathbf{p}| > \frac{\sqrt{3}}{\sqrt{2}(2 - \sqrt{3})} \approx 4.57.$$

then the  $D_c$  has radius greater than  $\sqrt{2}$  and such a lattice point exists. Note that this is a sufficient but not necessary condition on  $\mathbf{p}$ .

Checking the small number of  $\mathbf{p}$  values with  $|\mathbf{p}| < 4.57$  and  $\kappa$  odd there are appropriate lattice points  $\mathbf{a}$  for most such  $\mathbf{p}$ . The following table shows an appropriate value for  $\mathbf{a}$  for

most such  $\mathbf{p}$ , and “None” where no such  $\mathbf{a}$  exists.

(4.5)

$\mathbf{p}$	$(4, 1)^T$	$(3, 3)^T$	$(3, 2)^T$	$(3, 1)^T$	$(3, 0)^T$	$(2, 1)^T$	$(1, 1)^T$	$(1, 0)^T$
$\mathbf{a}$	$(1, -2)^T$	$(1, -1)^T$	$(1, -2)^T$	$(1, -2)^T$	$(0, 2)^T$	None	None	None

For reflections/rotations of these values of  $\mathbf{p}$  the corresponding reflection/rotation of  $\mathbf{a}$  is an appropriate choice.

Thus for all  $\mathbf{p} = (p_1, p_2)^T$  such that  $\kappa = \gcd(p_1, p_2)$  except

$$(4.6) \quad \mathbf{p} = \begin{pmatrix} 1 \\ 0 \end{pmatrix}, \begin{pmatrix} 1 \\ 1 \end{pmatrix}, \begin{pmatrix} 1 \\ 2 \end{pmatrix}$$

and reflections and rotations of these, there is a choice of  $\mathbf{a}$  so that the conditions of Theorem 2 is satisfied when  $N = \frac{(2A+1)\kappa-1}{2}$  for any  $A \in \mathbb{N}$  such that  $A > \frac{2|\mathbf{p}|^2-\kappa}{2\kappa}$ .  $\square$   $\square$

**Theorem 4.3.** *The steady state  $\Omega^* = 2\Gamma \cos(\mathbf{p} \cdot \mathbf{x})$  is nonlinearly unstable for all  $\mathbf{p} = (p_1, p_2)^T$  except possibly*

- $p_1 \equiv p_2 \equiv 0 \pmod{2}$ ;
- $\mathbf{p} = (\pm 1, \pm 0)^T$ ;
- $\mathbf{p} = (\pm 0, \pm 1)^T$ ;
- $\mathbf{p} = (\pm 1, \pm 1)^T$ ;
- $\mathbf{p} = (\pm 2, \pm 1)^T$ ;
- $\mathbf{p} = (\pm 1, \pm 2)^T$ .

*Proof.* By Lemma 4.2, for all  $\mathbf{p}$  except those listed above there exists some  $\mathbf{a}$  such that  $\rho_0 < 0$  and  $\rho_0 + \rho_2 < 0$  (or  $\rho_0 + \rho_{n-2} < 0$ ) for an appropriate choice of  $N$ . Thus by Theorem 3.4 there exists a real positive eigenvalue. Moreover, the eigenvalue is greater than  $\sqrt{-\rho_1(\rho_0 + \rho_2)}$  (or  $\sqrt{-\rho_{n-1}(\rho_0 + \rho_{n-2})}$ ) which is both positive and independent of the choice of truncation size  $N$ . The truncation size  $N$  can be increased without bound, by Lemma 4.1. Hence there is a hyperbolic eigenvalue in the limit  $N \rightarrow \infty$  and the spectrum of the PDE is unstable.

Linear instability follows from this and the result in [11], which shows that the spectral mapping theorem holds. To conclude nonlinear instability we appeal to the work of Friedlander, Strauss and Vishik [8], Shvidkoy and Latushkin [18], and Lin, Wang, and Zhang [13]. In [8] it was shown that sufficient conditions for nonlinear instability are linear instability together with a ‘spectral gap’ condition. In [18] it was shown that the essential spectrum of the linearised Euler operator in the cases we are considering is  $i\mathbb{R}$ . Because of the presence of a point of discrete spectrum off the imaginary axis, we have a spectral gap, and hence nonlinear instability.  $\square$   $\square$

Note that this does *not* preclude the possibility that the values of  $\mathbf{p}$  listed as exceptions do not also lead to a linearly unstable steady state  $\Omega^*$ . In fact, for  $\mathbf{p} = (1, 1)^T, (2, 1)^T$  and reflections/rotations thereof numerical results find non-zero non-imaginary eigenvalues. For  $\mathbf{p} = (1, 1)^T$  there is one complex quadruplet of eigenvalues,  $\pm 0.24822 \pm 0.35172i$  to five decimal places, calculated with  $N = 1500$  and  $\Gamma = 1$ . For  $\mathbf{p} = (2, 1)^T$  there are two real pairs and two complex quadruplets of eigenvalues. Numerical results also show that for  $p_1 \equiv p_2 \equiv 0 \pmod{2}$ ,  $\Omega$  is also unstable.

Theorem 4.3 together with the numerical results mentioned and the spectral mapping theorem shown in [8] indicate that the only linearly stable equilibrium of type (1.2) is  $\mathbf{p} = (\pm 1, \pm 0)^T, (\pm 0, \pm 1)^T$ , because only these have the single lattice point  $\mathbf{a} = (0, 0)^T$  inside the unstable disc. This exceptional case leads only to zero eigenvalues. All lattice points outside the unstable disc (including those on the boundary) do not contribute to instability (see section 3.1) and hence this equilibrium is spectrally stable. By [10] it is then linearly stable. According to Arnol'd [3] and Li [12] it is also Lyapunov stable.

We can compare this to the results described in [4]. For the Navier-Stokes equation with non-zero viscosity, they show that the solution

$$(4.7) \quad \Omega(x, y, t) = e^{-\nu t} \cos(x)$$

is ‘metastable’, in the sense that it decays on a slow, viscous timescale. If we let  $\nu = 0$  (no viscosity), this is the same as our equilibrium with  $\mathbf{p} = (1, 0)^T$ .

## 5. SOME NUMERICAL RESULTS

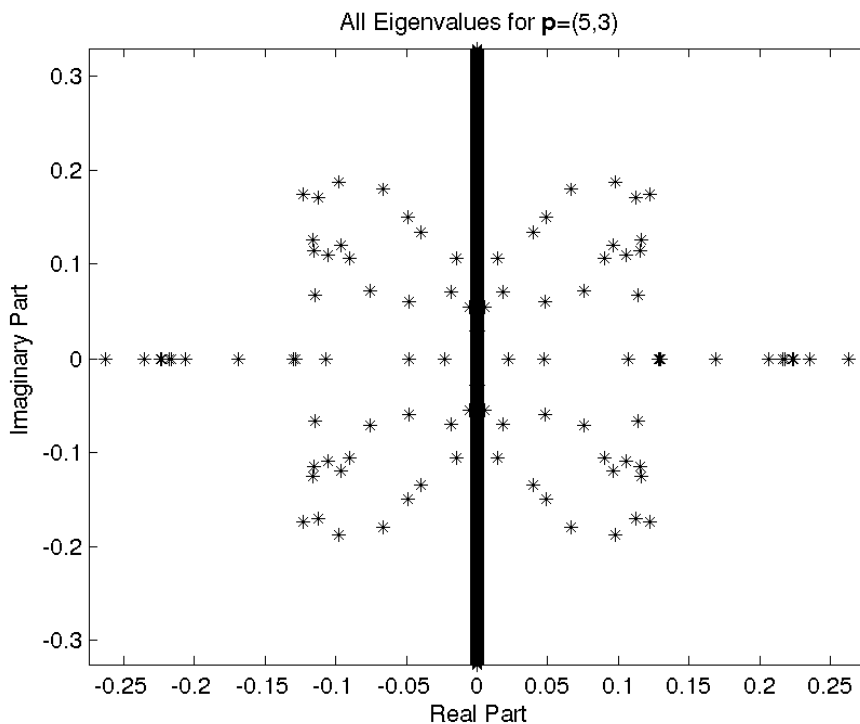


FIGURE 5.1. All eigenvalues for the case  $\mathbf{p} = (5, 3)^T$ ,  $\Gamma = \frac{1}{2}$ . The Zeitlin truncation is used with  $N = 200$ . Note there are 200 (or 100 plus-minus pairs) eigenvalues with non-zero real part, and there are 100 interior lattice points in  $D_{\mathbf{p}} \setminus \{\mathbf{0}\}$ . This confirms the result from [11]. Of the non-imaginary eigenvalues, 56 are real and 144 are complex. The number of interior points that satisfy  $\rho_0 < 0$ ,  $\rho_1, \rho_{-1} > 0$  is 24. All these points correspond to real pairs (two sets of  $24 = 48$ ). The other real pairs come from interior points with  $\rho_0 < 0$  and  $\rho_1 < 0$  or  $\rho_{-1} < 0$ . This usually creates a complex quadruplet but in a few cases corresponds to two real pairs instead. Increasing  $N$  does not change the number of non-imaginary eigenvalues.

**5.1. The Unstable Spectrum.** The class decomposition means that we now compute the eigenvalues of  $(2N + 1)$  matrices, each of size  $(2N + 1) \times (2N + 1)$ . Without the class decomposition, the eigenvalues of one  $(2N + 1)^2 \times (2N + 1)^2$  matrix need to be computed. So the class decomposition results in an extremely significant saving of computation time.

Figure 5.2 shows the values at which the calculated eigenvalues converge as a function of the size  $N$  of our truncation domain  $\mathcal{D}$ . Compared to a Galerkin truncation the eigenvalue converges for much smaller values of  $N$  when using Zeitlin's method.

Figure 5.3 shows the correspondence between the location of values of  $\mathbf{a}$  and the types of eigenvalues of the class  $\Sigma_{\mathbf{a}}$ . This corresponds to the results of Section 3. Compare the positioning of the Fourier modes with Figure 3.1.

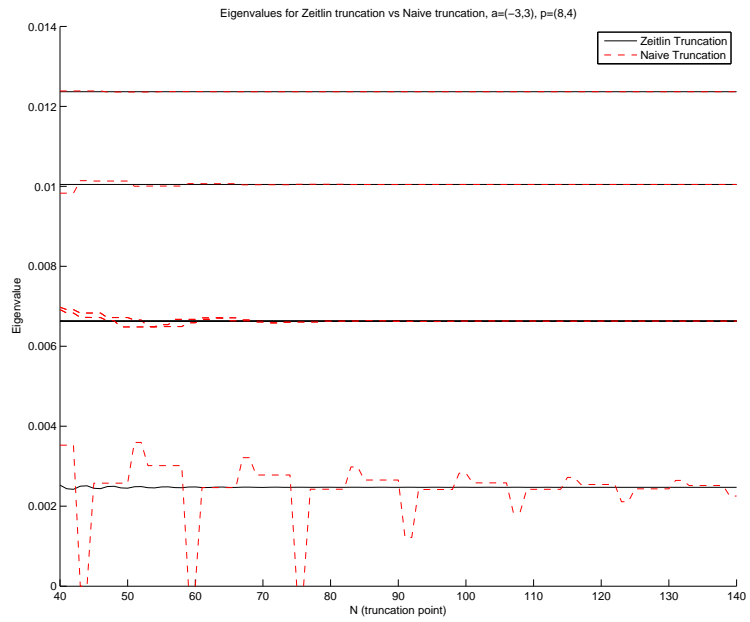
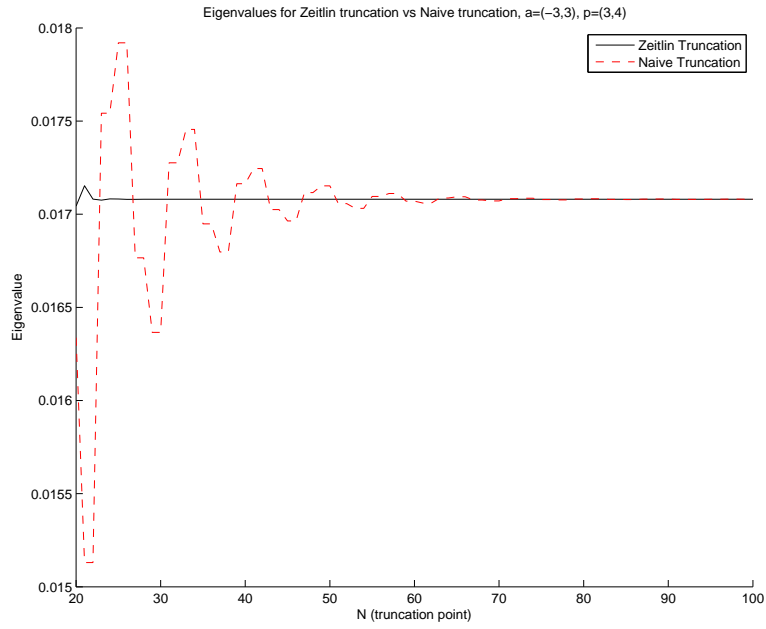


FIGURE 5.2. See following page.

FIGURE 5.2. Numerically computed real eigenvalues vs Fourier mode domain size  $N$ . For the top figure,  $\mathbf{a} = (-3, 3)^T$  and  $\mathbf{p} = (3, 4)^T$ . For the bottom figure,  $\mathbf{a} = (-3, 3)^T$  and  $\mathbf{p} = (8, 4)^T$ . For both figures,  $\Gamma = 1$ . The dashed red lines show the eigenvalues computed by the Galerkin truncation in equation (2.24), and the full black lines show the eigenvalues computed by the Zeitlin truncation in equation (2.23). For this figure Theorem 3.1 is applicable so there is exactly one pair of real eigenvalues. The convergence of the eigenvalue computed with the Zeitlin truncation is much faster and smoother. In the bottom figure, because  $\gcd(p_1, p_2) > 1$  there are multiple eigenvalues with non-zero real part, resulting from when the class wraps around on itself as discussed in section 4. However, Zeitlin's truncation still computes the expected eigenvalues correctly and more accurately than the naïve truncation. Note that these plots take the limit of the factor of  $\alpha$ , so the convergence is clearer.

Figure 5.1 shows all the eigenvalues associated with  $\mathbf{p} = (5, 3)^T$  for a truncation value  $N = 200$ . There are 200 eigenvalues with non-zero real part which is exactly twice the number of interior lattice points in  $D_{\mathbf{p}} \setminus \mathbf{0}$ . This agrees with the result in [11] that the discrete spectrum of the corresponding operator has at most  $2|D_{\mathbf{p}}| - 2$  non-imaginary eigenvalues. Our numerical results indicate that this bound is sharp; for all choices of  $\mathbf{p}$  tested there is equality.

Figure 5.4 shows the lower bound (3.22) and the numerically calculated maximum real eigenvalue across a range of values of  $\mathbf{p}$ . For this figure we vary  $p_1$  and let  $\mathbf{p} = (p_1, 1)^T$  and  $\mathbf{a} = (-1, \lfloor p_1/2 \rfloor)^T$ . It appears that our lower bound is a reasonable approximation to the actual eigenvalue but not particularly close. This is fine, as the bound is only intended to be greater than zero.

Figure 5.5 shows the real parts of the eigenvalues as a function of the distance of the class  $\Sigma_{\mathbf{a}}$  from the class  $\Sigma_{\mathbf{0}}$  for a fixed  $\mathbf{p}$  and  $N$ . Of particular note is that the real parts of the complex eigenvalues seem to have a relatively smooth correlation with this distance. The eigenvalues with largest real parts roughly correspond to lattice points  $\mathbf{a}$  that are partway between  $\Sigma_{\mathbf{0}}$  and the boundary of  $D_{\mathbf{p}}$ .

**5.2. The Stable Spectrum.** Figure 5.6 shows the density of the imaginary parts of the spectrum for  $\mathbf{a} = (-4, 7)^T$ ,  $\mathbf{p} = (7, 5)^T$ . There are also non-imaginary eigenvalues but these are not shown on the figure.

For any  $\varepsilon > 0$ , we can choose  $N$  so that there is some class  $\Sigma_{\mathbf{a}}$  such that  $\frac{1}{|\mathbf{p}|^2} < \varepsilon$  for all  $\mathbf{b} \in \Sigma_{\mathbf{a}}$ . So the imaginary spectrum of this class can be approximated by taking  $\rho_k \approx \frac{1}{|\mathbf{p}|^2}$ . The resulting matrix  $A$  from (2.23) is now circulant. A circulant matrix is diagonalised by a discrete Fourier transform [9]. Thus the eigenvalues of  $A$  are then found to be

$$(5.1) \quad \lambda_j = \frac{2i}{|\mathbf{p}|^2} \sin\left(\frac{2\pi j}{n}\right) \text{ for } j = 0, \dots, n-1 \text{ where } j \text{ is the size of } A.$$

See [9] for details of this calculation.

Thus the approximate imaginary spectrum of  $\Sigma_{\mathbf{a}}$  for sufficiently large  $|\mathbf{a}|$  lies in the interval  $\frac{2i}{|\mathbf{p}|^2}[-|\alpha|, |\alpha|]$  on the imaginary axis. Taking the limit  $N \rightarrow \infty$  (and so  $n \rightarrow \infty$ ), for each  $x \in [0, 1]$  there is a correspondence with an eigenvalue  $\lambda_x$  where  $x =$

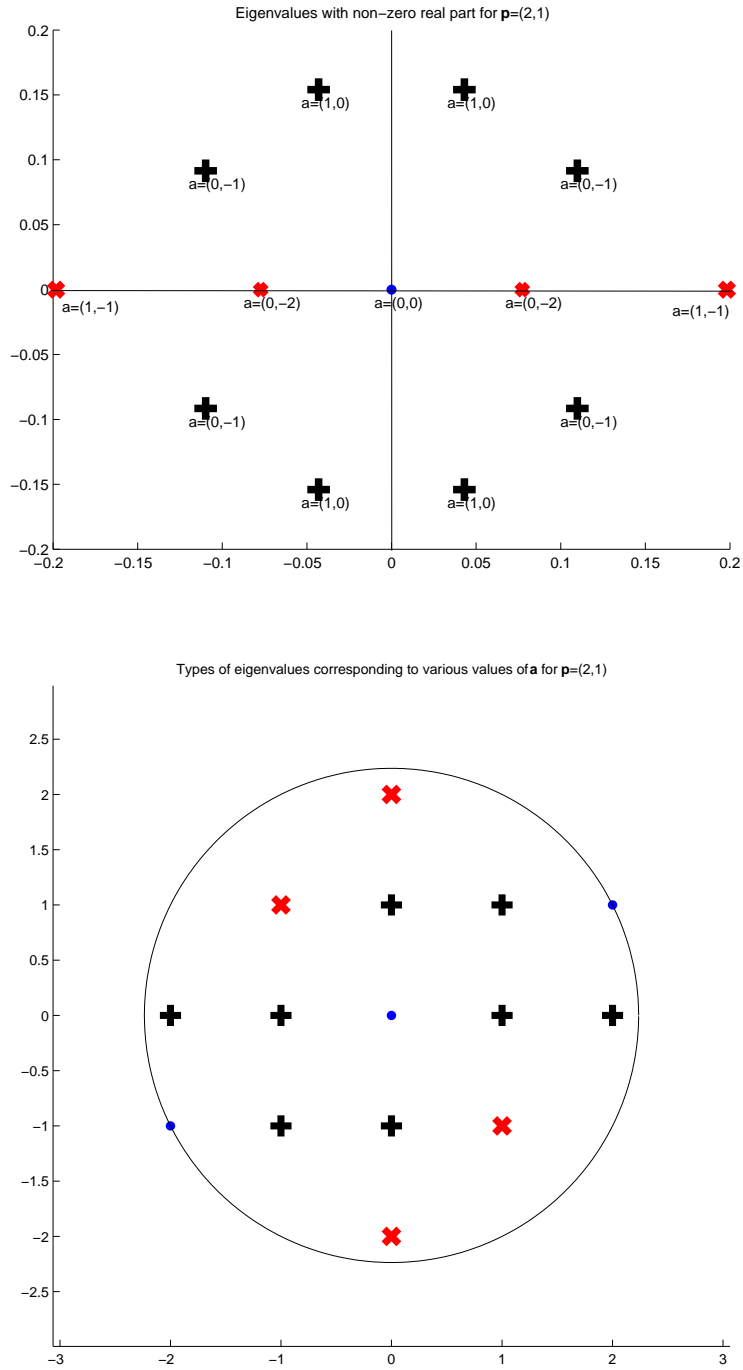


FIGURE 5.3. See following page.

FIGURE 5.3. Non-imaginary eigenvalues (top) and the corresponding lattice points  $\mathbf{a}$  in the unstable disc (bottom) for the equilibrium with  $\mathbf{p} = (2, 1)^T$ . At the top, the eigenvalues with non-zero real part for every unstable class  $\Sigma_{\mathbf{a}}$  are shown. Eigenvalues with zero imaginary part are marked with a red  $\times$ , complex eigenvalues are marked with a black  $+$ , and the zero eigenvalues are marked with a blue circle. In the bottom figure we see the values of  $\mathbf{a}$  that correspond to these classes. The zero class led by  $\mathbf{a} = (0, 0)^T$  gives only zero eigenvalues. Compare the locations of the classes corresponding to real eigenvalues to Figure 3.1. For these figures,  $\Gamma = \frac{1}{2}$ , so  $\Omega^* = \cos(\mathbf{x} \cdot \mathbf{p})$ .

$\frac{1}{2\pi} \sin^{-1} \left( \frac{\lambda_x |\mathbf{p}|^2}{2i} \right)$ . Differentiating this gives the density function

$$(5.2) \quad F(x) = \frac{|\mathbf{p}|^2}{\pi \sqrt{4\alpha^2 - |\mathbf{p}|^4 x^2}}.$$

That is, the proportion of the eigenvalues lying between  $c_1 i$  and  $c_2 i$  on the imaginary axis is  $\int_{c_1}^{c_2} F(x) dx$  for  $c_1, c_2 \in \frac{2}{|\mathbf{p}|^2} [-|\alpha|, |\alpha|]$ . This curve is also plotted in 5.6, and it agrees well with the numerically calculated eigenvalues. This is surprising as the choice of  $\mathbf{a}$  for the numerically calculated eigenvalues does not have a particularly high value of  $|\mathbf{a}|$ . We can conclude that equation (5.2) gives a reasonable approximation of the imaginary spectrum for many choices of  $\mathbf{a}$ .

Latushkin et. al. [11, 18] describe the essential spectrum of the linearised operator that coincides with our limit  $N \rightarrow \infty$ . The essential spectrum for the class led by  $\mathbf{a}$  is given in that paper as

$$(5.3) \quad \sigma_{\text{ess}} = i[-|\beta|, |\beta|], \text{ where } \beta = \frac{2}{|\mathbf{p}|^2} (\mathbf{a} \times \mathbf{p}) \Gamma.$$

In the limit  $N \rightarrow \infty$ ,  $\frac{\sin(\varepsilon \mathbf{a} \times \mathbf{p})}{\varepsilon} \rightarrow \mathbf{a} \times \mathbf{p}$ , so  $\frac{2}{|\mathbf{p}|^2} |\alpha| \rightarrow |\beta|$ . Thus our approximation for large  $N$  reproduces the essential spectrum of a single class calculated in [11]. Note that this is the essential spectrum associated with a single subsystem of the linearised problem. The essential spectrum of the full system is the superposition of all these essential spectra. It was shown in [18] that this is  $i\mathbb{R}$ , which follows from considering the superposition of (5.3) for all possible values of  $\mathbf{a}$ .

## 6. CONCLUSION

We have demonstrated the linear instability of the stationary solutions with vorticity  $\Omega^* = 2\Gamma \cos(\mathbf{p} \cdot \mathbf{x})$  in the Euler equations for all values of  $\mathbf{p}$  such that  $\gcd(p_1, p_2)$  is not even and  $\mathbf{p} \neq (1, 0)^T$  (or rotations and reflections thereof). In doing so we have also shown the numerical and analytical advantages of Zeitlin's truncation scheme. However, such a scheme has limitations, particularly regarding the decomposition of the problem into subsystems. Namely, that the truncation creates unexpected and unwanted side effects in the case that  $\gcd(p_1, p_2)$  is even.

We have also recreated and extended a number of results described by Li [12] and Latushkin, Li, and Stanislavova [11], and Shvidkoy and Latushkin [18]. Specifically, we have shown that the "unstable disc theorem" presented in [12] still holds true in the

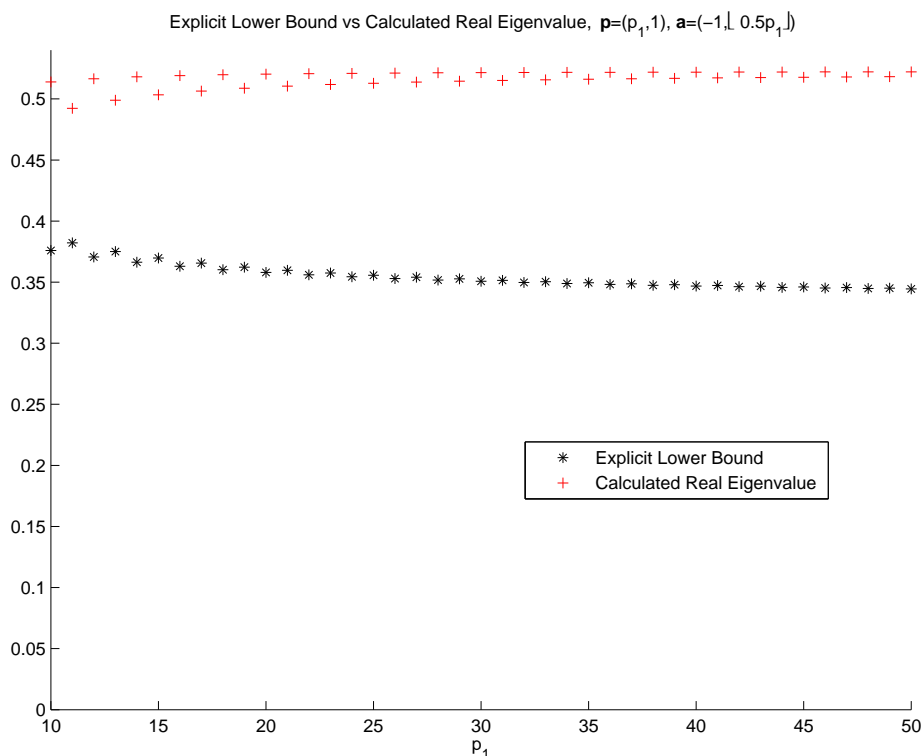


FIGURE 5.4. The lower bound given by (3.22) (black \*) vs the maximum calculated eigenvalue (red +) for a variety of values of  $\mathbf{p}$ . We look at  $\mathbf{p} = (p_1, 1)^T$ ,  $\mathbf{a} = (-1, [0.5p_1])$  and vary  $p_1$  along the  $x$  axis. These values of  $\mathbf{a}$  will satisfy the condition in Figure 3.1, guaranteeing a real eigenvalue. For the calculated eigenvalues a truncation size of  $N = 2000$  is used. For the lower bounds the choice of  $N$  is irrelevant. The  $\alpha$  factor is applied after taking the limit  $\alpha \rightarrow \Gamma \mathbf{a} \times \mathbf{p}$ .  $\Gamma = 1$  for this figure.

current context of finite dimensional approximation. Moreover, we have shown that for almost all  $\mathbf{p}$  we can use the unstable disc to prove instability (as opposed to stability, which is what Li has done). We have also numerically verified the bound on the number of non-imaginary eigenvalues and the essential spectrum of an individual class in [11] and [18]. We used very different approaches and arguments to those papers.

There are two obvious extensions of the work presented in this paper. The first is a complete description of the non-imaginary spectrum. This would require first showing that for two consecutive negative values of  $\rho$ , the corresponding subsystem has four non-imaginary eigenvalues, either two real pairs or a complex quadruplet. This could culminate in the statement that there are exactly as many unstable eigenvalue pairs as there are lattice points inside the unstable disc, sharpening the results from [11]. Numerically this is what we observe.

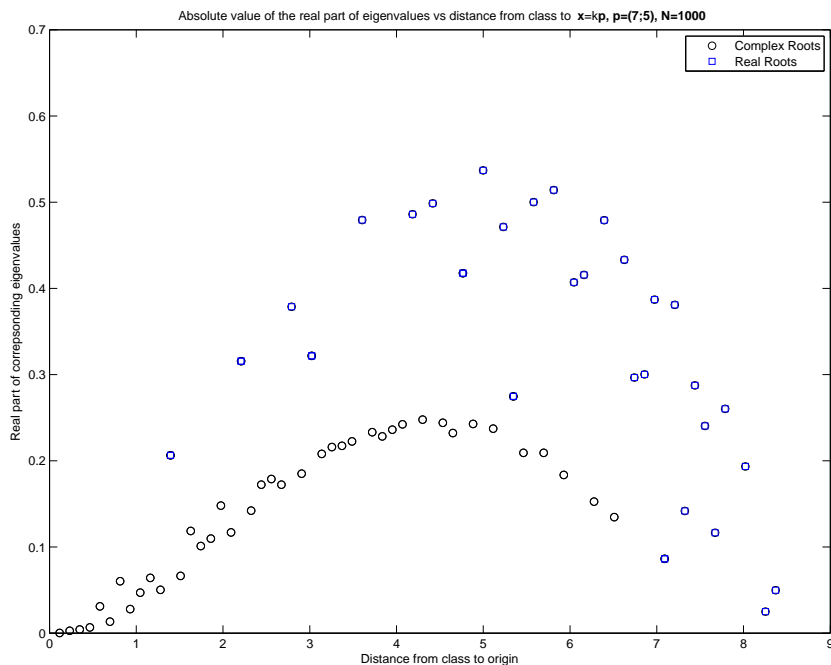


FIGURE 5.5. The real part of all eigenvalues with non-zero real part, plotted against the perpendicular distance of the class from  $\Sigma_0$ . The eigenvalues with zero imaginary part are marked in blue, and the eigenvalues with non-zero imaginary part are marked in black. For this plot  $\mathbf{p} = (7, 5)^T$ ,  $\Gamma = 1$ , and  $N = 1000$ .

The other extension would be a description, or an explanation, of the cases for  $\mathbf{p}$  that our method cannot analyse. This could possibly arise from a different choice of algebra for the Poisson bracket or an alteration of Zeitlin's existing algebra. It would also be interesting to see if any of the methods used in this paper could be applied to more complex steady states; for instance  $\Omega^* = \sin(p_1 x) \sin(p_2 y)$ .

#### ACKNOWLEDGEMENTS

RM gratefully acknowledges M. Beck and Y. Latushkin for extremely helpful discussions on the known stability results on the 2D Euler equations.

#### REFERENCES

- [1] Arnold, V.: Sur la géométrie différentielle des groupes de lie de dimension infinie et ses applications à l'hydrodynamique des fluides parfaits. In: Annales de l'institut Fourier, vol. 16, pp. 319–361. Institut Fourier (1966)
- [2] Arnold, V.: Mathematical Methods of Classical Mechanics. Springer (1978)
- [3] Arnold, V., Khesin, B.A.: Topological Methods in Hydrodynamics. Springer (1998)

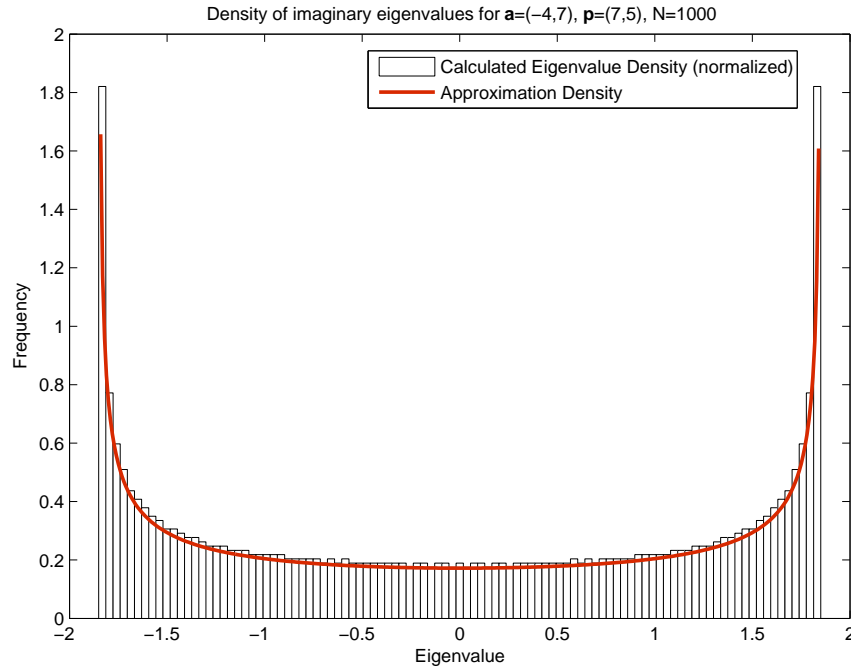


FIGURE 5.6. The imaginary part of the spectrum, for the class  $\mathbf{a} = (-4, 7)^T$ ,  $\mathbf{p} = (7, 5)^T$ ,  $\Gamma = 1$ . The bars show the normalized density of the imaginary eigenvalues computed for  $N = 1000$ . The red line shows the approximate density computed by taking the approximation  $\rho_k \rightarrow \frac{1}{|\mathbf{p}|^2}$ , which holds for large values of  $|\widehat{\mathbf{a} + k\mathbf{p}}|$ . In this approximation the matrix is a circulant and so these eigenvalues can be calculated explicitly by (5.2). For this figure  $\Gamma = 1$ .

- [4] Beck, M., Wayne, C.E.: Metastability and rapid convergence to quasi-stationary bar states for the two-dimensional navier-stokes equations. *Proceedings of the Royal Society of Edinburgh Section A - Mathematics* **143**(5), 905–927 (2013)
- [5] Belenkaya, L., Friedlander, S., Yudovich, V.: The unstable spectrum of oscillating shear flows. *SIAM Journal on Applied Mathematics* **59**(5), 1701–1715 (1999)
- [6] Butta, P., Negrini, P.: On the stability problem of stationary solutions for the Euler equation on a 2-dimensional torus. *Regular and Chaotic Dynamics* **15**(6), 637–645 (2010)
- [7] Favard, J.: Sur les polynomes de Tchebicheff. *Comptes Rendus de l'Académie des Sciences* **200**, 2052–2053 (1936)
- [8] Friedlander, S., Strauss, W., Vishik, M.: Nonlinear instability in an ideal fluid. In: *Annales de l'Institut Henri Poincaré (C) Non Linear Analysis*, vol. 14, pp. 187–209. Elsevier (1997)
- [9] Karner, H., Schneid, J., Ueberhuber, C.W.: Spectral decomposition of real circulant matrices. *Linear Algebra and its Applications* **367**, 301–311 (2002)
- [10] Kolev, B.: Poisson brackets in hydrodynamics. *Discrete and Continuous Dynamical Systems* **19**, 555–574 (2007)
- [11] Latushkin, Y., Li, Y.C., Stanislavova, M.: The spectrum of a linearized 2D Euler operator. *Studies in Applied Mathematics* **112**, 259–270 (2004)

- [12] Li, Y.C.: On 2D Euler equations. I. On the energy-casimir stabilities and the spectra for linearized 2D euler equations. *Journal of Mathematical Physics* **41**(2), 728 – 758 (2000)
- [13] Lin, Z., Wang, Z., Zeng, C.: Stability of traveling waves of nonlinear Schrödinger equation with nonzero condition at infinity. arXiv preprint arXiv:1405.2583 (2014)
- [14] Meshalkin, L., Sinai, I.G.: Investigation of the stability of a stationary solution of a system of equations for the plane movement of an incompressible viscous liquid. *Journal of Applied Mathematics and Mechanics* **25**(6), 1700–1705 (1961)
- [15] Newton, P.K.: *The N-Vortex Problem: Analytical Techniques*. Springer (2001)
- [16] Pope, C.N., Romans, L.J.: Local area-preserving algebras for two-dimensional surfaces. *Classical and Quantum Gravity* **7**, 97–109 (1990)
- [17] Ray, S.S., Frisch, U., Nazarenko, S., Matsumoto, T.: Resonance phenomenon for the Galerkin-truncated Burgers and Euler equations. *Physics Review E* **84** (2011)
- [18] Shvidkoy, R., Latushkin, Y.: The essential spectrum of the linearized 2d euler operator is a vertical band. *Contemporary Mathematics* **327**, 299–304 (2003)
- [19] da Silva, A.C.: *Lectures on Symplectic Geometry*. Springer (2001)
- [20] Szegő, G.: *Orthogonal Polynomials*. American Mathematical Society (1939)
- [21] Zeitlin, V.: Finite-mode analogs of 2D ideal hydrodynamics: Coadjoint orbits and local canonical structure. *Physica D: Nonlinear Phenomena* **49**(3), 353–362 (1991)
- [22] Zeitlin, V.: On self-consistent finite-mode approximations in (quasi-)two-dimensional hydrodynamics and magnetohydrodynamics. *Physics Letters A* **339**, 316–324 (2005)